A Generalized Telerobotic Hand Controller for Force Reflection

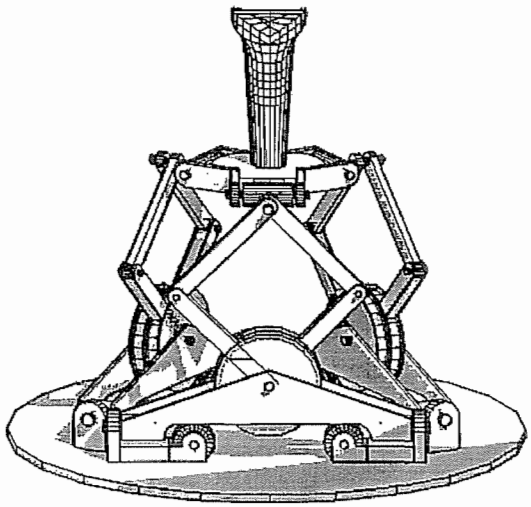

GREGORY L. LONG
Assistant Professor

CURTIS L. COLLINS
Graduate Student

University of California, Irvine
Mechanical and Aerospace Engineering
Irvine, California 92717

A Final Report to the
California Department of Transportation/University of California, Davis
Advanced Highway Maintenance Technology Program

March 1, 1993

UCD-ARR-93-03-01-01

Contents

1 Introduction

Future strategies for environmental clean-up and hazardous waste removal will rely primarily on remote manipulation and sensing. Remote manipulation via a computer controlled electro-mechanical system is known as *telerobotics.* During the past decade, computationally efficient algorithms and inexpensive computers have provided an enhanced framework for telerobotic development. With increased computational power and sophisticated programming languages, the addition of high-performance generalized hand controllers has expanded the versatility of telerobotic systems.

This report describes various components of a newly developed generalized telerobotic hand controller. The hand controller was designed and fabricated in the Robotics Laboratory at the University of California, Irvine. While these efforts have focused primarily on the feasibility of new telerobotics technology, attention has been given to potential commercial applications. The generalized controller was developed under contract with the California Department of Transportation/University of California, Davis Advanced Highway Maintenance Technology program.

In this report, we first provide an overview of the UC Irvine Telerobotic System. After this overview, various system components, including hardware, software, and analyses, are then described in Sections 3, 4, and 5. Several system extensions are informally discussed in Section 6, while mechanical component drawings are included in the appendix.

2 Overview of UC Irvine Telerobotic System

2.1 Motivation

The generalized telerobotic hand controller described in this report is part of a larger electromechanical system comprised of a radio-controlled robotic arm module with appropriate end-effectors. This robotic system is currently planned for remote handling and solid debris removal from the highways, as well as other highway maintenance operations. In addition, the system will have the enhanced capability of chemical sampling and emergency clean-up of dangerous spills.

As the system has been designed for "short-range" teleoperation, we have not focused on time delays, predictive displays, special vision systems, and other complex interface devices/architectures inherent to remote teleoperation in undersea and outerspace. We have assumed the remote site can be visually observed with the human eye or with a simple television system.

To facilitate control over all performance factors and design criteria, we have carefully

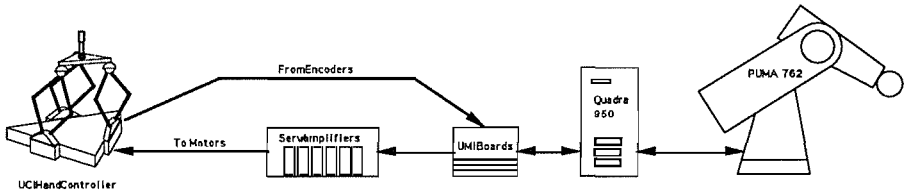

Figure 1: Schematic Representation of UC Irvine Telerobotic System

chosen the various mechanical and electrical components. Throughout the entire design process, we have used proven technologies as building blocks for the final system. We have acquired reliable and modular commercial products to provide a standard low level interface for computer control. This standard interface allows an operator to quickly change an existing component with other control devices.

2.2 System Hardware

The existing telerobotics system consists of the five subsystems shown in Figure 1. The generalized hand controller, a powered servo amplifier unit, nuLogic motion control and signal interface boards, a Quadra 950, and a PUMA 762 robot manipulator. The hand controller is interfaced with Universal Motion Interface (UMI) boards to the Quadra 950 containing the nuLogic motion control boards. The servo amplifiers are used to drive six direct current servo motors located on the generalized hand controller's base.

2.2.1 Generalized Hand Controller

Our primary focus was to design the six degree-of-freedom hand controller shown in Figure 2. A comparison of existing controller designs, as well as performance specifications have been documented by Fischer, Daniel, and Siva [1990]. Based on the performance specifications of Fischer, et. al., and the original pantograph design of Inoue, Tsusaka, and Fukuizumi [1986], we have developed a parallel platform generalized hand controller that is displaced by three pantograph linkages. In Long and Collins [1992] we present the control relationships needed for position and rate control, as well as force feedback to an operator (note: these developments are given in Section 5 of this report).

2.2.2 Servo Amplifiers

The six DC servo motors are each driven by its own pulse-width-modulated (PWM) servo amplifier. The six amplifiers are configured for a current mode with a flat open loop response. They are powered by a switching power supply. The servo amps and power supply are

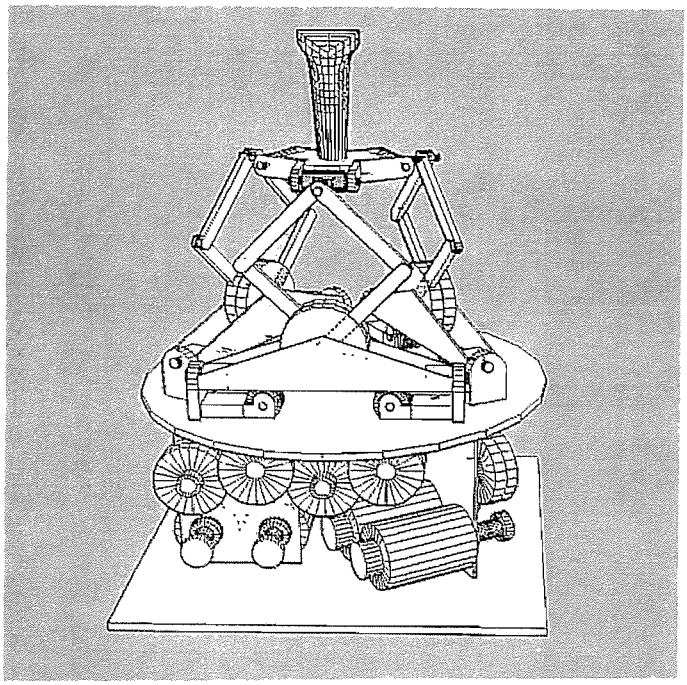

Figure 2: UC Irvine Generalized Hand Controller

efficient, reliable, and stable. These particular sub-components can be upgraded to brushless DC drives in order to enhance future prototypes.

2.2.3 nuLogic Interface

All encoder inputs and servo amplifier command outputs are interfaced with nuLogic's motion control boards through the company's Universal Motion Interface (UMI) boards. These interface boards provide the necessary connections, filters, and buffers for signals to and from the Quadra 950.

Two nuControl boards and one nuPosition board are installed on the NuBus of the Quadra 950. nuControl is a programmable three-axis motion controller. The command signal to the servo amplifiers is generated by the nuControl boards, which provide a PID controller using encoder feedback for each axis. The nuPosition board is used to read three extra encoders used for the kinematics calculations. All three boards have six TTL logic bits that can be configured as inputs or outputs. These TTL logic bits enable the servo amplifiers and also monitors their status.

2.2.4 Quadra 950

A Quadra 950 is used as the central processing unit for this system. Encoder information is received from the nuLogic boards through the NuBus interface. Command signals are sent

to the nuControl boards on the NuBus to direct the motion of the generalized controller. Data packets are sent through the Quadra's serial port for external robot control. High level commands are generated in the telerobotic system software which is written in the LabVIEW programming language G.

2.2.5 Puma 762

A Puma 762 was used to demonstrate the telerobotic system controller. The Puma 762 is controlled with the VAL II Mark III software developed by Unimation. VAL II provides complete control of all robot functions. In addition, there are two communication ports set up for supervisory functions and system control from an external computer. In this project, we have used the Alter Port facility for demonstration of resolved unilateral position control.

3 Motion Control Software: LabVIEW 2

The LabVIEW 2 software, produced by National Instruments, provides a menu driven graphical environment for constructing operator interfaces and developing programs in block diagram form. The LabVIEW 2 software provides mouse driven controls and displays, and a host of graphical elements that direct program flow. Programs constructed under LabVIEW 2 are converted into compiled code and executed under a data driven protocol. Modular programming is fully supported and code resources written in other standard programming languages (e.g., BASIC, C, and Fortran) can be linked within a LabVIEW 2 program.

The LabVIEW 2 software is currently available on Macintosh and MS DOS platforms. For these two platforms, there appears to be no difference in LabVIEW's operation; our choice of the former platform was based on positive experience with other Macintosh applications. The Macintosh LabVIEW 2 application is well supported by National Instruments and other software/hardware vendors. Currently, there are numerous data acquisition and control boards available for the NuBus as well as controllers conforming to the IEEE-488 standards. The Macintosh can be interfaced to the VXIbus system which is based on the VMEbus standard, allowing it to control other high-performance instrumentation.

3.1 Graphical Interface

LabVIEW 2 programs are called virtual instruments (VIs). The virtual instruments "mimic the time proven interface of hardware instrumentation" in software. LabVIEW 2 programs consist of two fundamental components: 1) a Front Panel and 2) a Block Diagram. A front panel is readily constructed using graphical depictions of familiar analog instrumentation such as buttons, switches, sliders, LEDs, character displays, and strip chart displays. All

front panel elements are program linked and act as either user inputs or display outputs from some program function.

The block diagram acts as the program. Block diagrams consist of graphical program elements connected by lines to depict program flow similar to flow charts or engineering system diagrams. This graphical representation of system flow is easily understandable, and program additions and modifications are readily.

The pre-packaged front panel elements facilitate the creation of thorough and complete operator interfaces. All front panel elements can be customized by modifying their size, labels, and colors. The creation details of graphical units are hidden. This allows the programmer to focus on the layout and functionality of the virtual instrument.

3.2 Programming Features

LabVIEW 2 provides the features of conventional programming languages in graphical form. Data types, Arrays, and Structures found in C and other languages have analogs in LabVIEW 2 and are depicted with different colored lines and graphical constructs. For and While loops have graphical representations as do Case Structures and a host of common functions normally found in a programming library. Macintosh features like file dialogue, message boxes, and sound can be easily accessed. LabVIEW 2 programs are also compiled before execution.

Program execution follows a data driven format. A function is executed only when it receives all of its input data. In addition, functions that reside on the same block diagram level are executed similar to a multi-tasking system. Execution order is determined by the data flow. Consequently, while one function is waiting for data, another function can execute.

LabVIEW 2 also has an added measure of flexibility. It provides a function that allows the user to include external code written in a conventional programming language. This function links external code resources into LabVIEW 2. When a code resource is executed, no other code in LabVIEW 2 can execute except interrupt routines.

A LabVIEW 2 virtual instrument can be used as a functional element in another virtual instrument; therefore, virtual instruments can act as subroutines (or subVIs). Since a subVI is actually a stand-alone program, it can be tested, debugged, and used without any calling program. Hence, complete programs can have a hierarchical and modular structure like conventional programming languages.

An example of a simple VI that takes the average of two numbers is shown in Figure 3. The connector pane represents how this VI would appear if it were used as a subVI in another program.

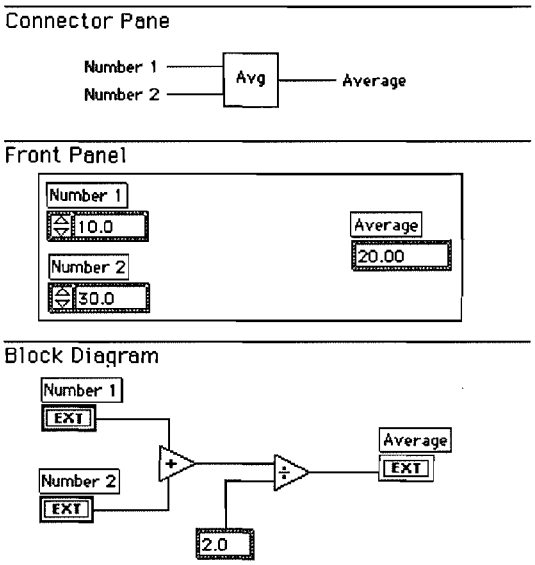

Figure 3: Representative Virtual Instrument

3.3 Virtual Instrument Libraries and Instrument Drivers

LabVIEW 2 has several libraries of standard virtual instruments. There are virtual instruments for acquiring and analyzing data, accessing the serial port, and controlling GPIB instrumentation. These virtual instruments provide a control level higher than the prepackaged functions.

For example, there is a library of virtual instruments tailored for use with the nuLogic motion control boards. There is a virtual instrument for each nuControl board command. In addition, there are high level virtual instruments for board initialization and for tuning the servo system parameters.

Another feature of the LabVIEW 2 software system is the availability of instrument drivers. These drivers are complete VIs for controlling specific instruments written by a manufacturer. These instruments conform to various control and communication standards. There are also industry-standard VXI instrument drivers.

4 Interface and Control of PUMA 762 Manipulator

A primary feasibility objective involved the successful implementation of a manual control strategy. This phase proved most challenging, as we were limited by several robot software and hardware specifications — in particular, the VAL II software incorporated with the Puma 762 robot manipulator. The Puma 762 manipulator is equipped with its own trajectory generation and joint control software, which are not intended for real-time teleoperation.

For approximately $4,500, a robot vendor, Advanced Robotics Research, will adapt existing software for teleoperation.

The software adaptation provided by Advanced Robotics Research permits direct communication with the joint servo amplifiers. In essence, direct communication by-passes the VAL II software and trajectory generator. Since VAL II is no longer in the communication loop, all joint trajectories, Cartesian trajectories, emergency, and fail-safe stops should be programmed and executed on an external computer. This particular implementation path would involve substantially more time than originally planned. For implementation on a Puma 762 manipulator, however, this is the path of choice.

After deliberately considering our options, we decided to use the Alter Port communication link located on the Puma 762 Unimation control panel. The Alter Port allows an external computer to "alter" the planned trajectory of the PUMA Robot. After numerous trials, we were able to successfully communicate with the Alter Port. Although the Alter Port link executes reasonably well for position control, it is not recommended for force control. For force control purposes, we suggest using a software "fix" similar to that provided by Advanced Robotics Research.

4.1 Communication System Overview

Initializing the communication link begins with the VAL II programming language and the Puma controller. The VAL II programming language is responsible for controlling the entire robot system by handling all high level status, error controls, and robot motion commands. Robot status and transformation information can be sent to an external computer from VAL II. In turn, motion information can be sent to VAL II from the external computer. This motion information is used to modify the robot arm trajectory. The alter mode is established with the ALTER command. The communication link and details of the information transfer protocol are described in Chapter 3 of the VAL II users manual.

The Alter Port and communication protocol allows an external computer to modify robot motions in real-time based on sensory information or an external computation. For our purposes, we desired robot motion only when commanded from the Quadra 950. Since the alter mode is functional only while the robot executes straight line motions, we utilized a fictitious infinite loop to move the end-effector.

After initializing alter mode, an alter starting message is immediately sent to the external computer. VAL II expects an answer within 250 ms or else it sends the alter starting message again. If the external computer does not respond after three alter starting messages, the VAL II program stops with an error. After alter mode is initialized, VAL II sends an alter running message about 30 times a second and expects the proper message from the external

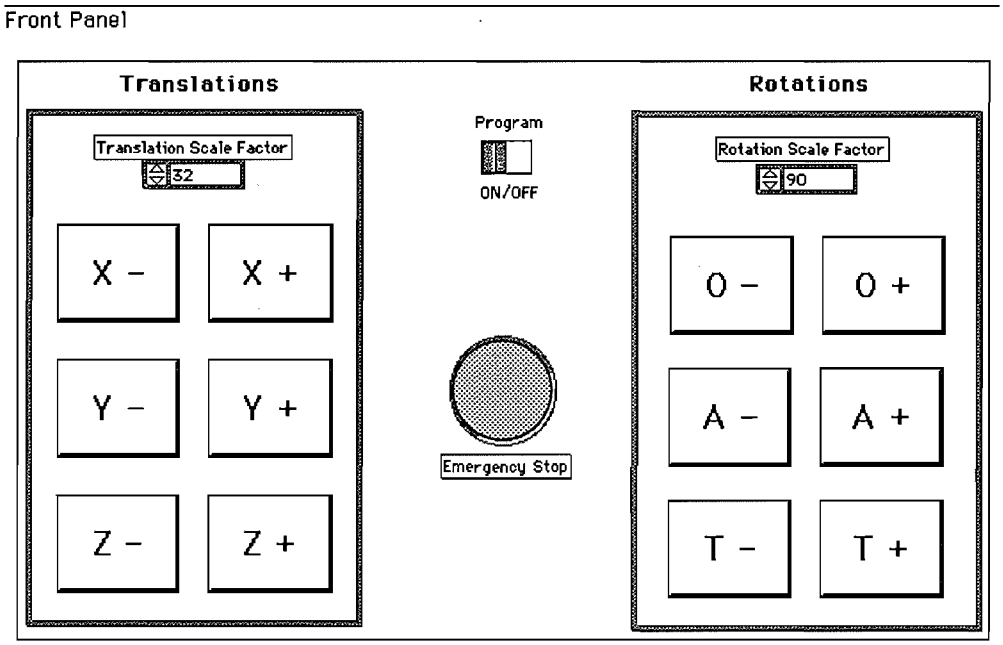

Figure 4: Front Panel of a Teach Pendant Virtual Instrument

computer.

Information packets are sent at 19200 baud over an RS-422 line. Each byte has 1 start bit and 1 stop bit with no parity. An information packet contains a message header, a string of data, a message trailer, and a checksum. The input data contains six 16 bit words sent in the order X, Y, Z displacement and ϕ_x, ϕ_y, ϕ_z rotation. The system permits motion in tool or world coordinates.

4.2 A LabVIEW Teach Pendant VI

To test the alter mode function available in VAL II, a Teach Pendant virtual instrument was constructed (Figure 4). Once the ALTER command is executed and the communication link established between VAL II and the Quadra 950, an operator can click and point the mouse to activate "buttons" causing the robot end-effector to move in the specified direction.

The virtual instrument front panel consists of 12 spring latch buttons, an E-Stop button, and a single switch. The 12 spring latch buttons correspond to positive/negative X, Y, Z displacement and ϕ_x, ϕ_y, ϕ_z rotation. The E-Stop causes VAL II to halt program execution. The switch stops the virtual instrument execution after the E-Stop.

A block diagram for this particular virtual instrument is shown in Figure 5. The entire diagram exists within an external sequence structure. This external structure forces the virtual instrument elements to execute sequentially instead of through the standard data

flow protocol. The last sequence frame contains a while loop in which the normal message from VAL II is read and a normal reply or alter message is sent to VAL II. The alter message sent to VAL II consists of the starting and stopping message bytes, plus the appropriate alter data and checksum required for the error checking protocol.

Each button is read and its state is converted into a motion command and checksum. Each button's boolean value is converted into its numeric representation and multiplied by a scale factor to obtain a move "distance." The scale factor controls the "distance" magnitude the robot is commanded to move every 28 ms.

4.3 Generalized Controller Interface

The generalized controller has six actively driven joints connected via cable transmissions to a corresponding motor. Attached to each motor is an encoder providing position feedback to a forward kinematics algorithm, as discussed in Section 5. The forward kinematics equations describe the position and orientation of the controller's top platform relative to its base. The forward kinematics formulation is simplified by attaching additional encoders to three passive joints, making nine the total number of joint encoder feedback.

The top platform's position and orientation relative to base is used to position control the Puma manipulator. This relative displacement information is inserted into an information packet, and then written to the serial port. The kinematic transformation and information process is achieved with three virtual instruments: an initial VI to read the nine joint angles, an intermediate VI to perform the forward kinematics, and a final VI to convert the result into a data packet.

The first VI utilizes the nuControl VIs as subVIs to access the motion control boards. The intermediate VI contains a Code Interface Node that sends joint angles to a code resource for computing the forward kinematics and thereby returning the top platform's Cartesian position and orientation. The final VI uses pre-packaged LabVIEW 2 conversion functions to first transform the results into a 16 bit integer, insert the integer into a data package, and finally write the data package to the serial port.

5 Generalized Hand Controller

In this section we discuss the kinematics and force control of the six degree-of-freedom generalized hand controller. The generalized hand controller is based on the parallel platform pantograph design introduced by Inoue, Tsusaka, and Fukuizumi [1986]. The original device introduced by Inoue, Tsusaka, and Fukuizumi was used as an actively compliant six degree-of-freedom wrist mechanism, attached to a serial-chain manipulator.

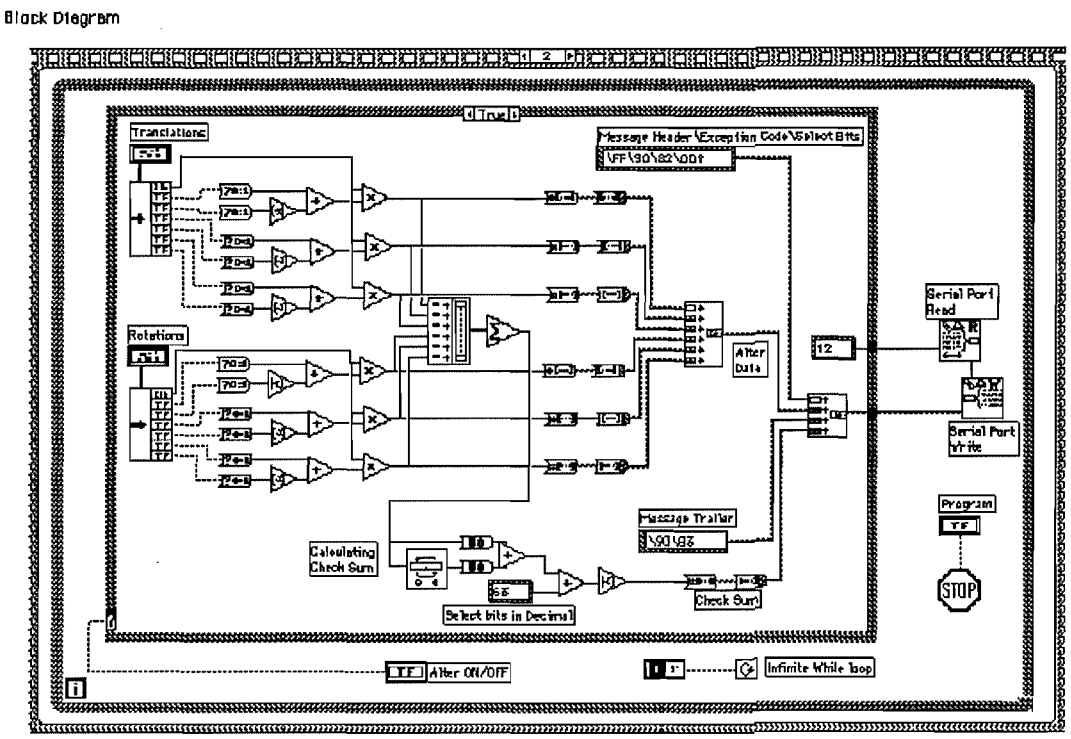

Figure 5: Selected Block Diagram from a Teach Pendant Virtual Instrument

A major difference between the generalized hand controller and Inoue's "parallel manipulator," however, is the generalized hand controller has a mechanical transmission comprised of cable/pulley reducers — the "parallel manipulator" has a planetary gear transmission. The change from planetary gears to cables and pulleys enhances transmission performance by minimizing friction, increasing efficiency, and eliminating backlash and torque ripple (see Salisbury [1987] and Townsend [1988]).

The device has three pantograph linkages, each attached to one mid-point of an equilateral base triangle through a passive revolute joint. At the opposite end, each pantograph is connected with one vertex of a top equilateral triangle through a three degree-of-freedom ball-in-socket joint.

Each pantograph linkage is comprised of two sub-chains denoted Left-chain and Right-chain as shown in Figure 6. For pantograph linkage i, $\theta_{2\mathrm{L},i}$ and $\theta_{2\mathrm{R},i}$ are the actuated variables, while $\theta_{1,i}$, $\theta_{3\mathrm{L},i}$, $\theta_{3\mathrm{R},i}$, and the ball-in-socket joint's degrees-of-freedom, are all passive variables.

5.1 Forward Kinematics

The top platform's position and orientation is obtained using the geometric construction shown in Figure 7. The top vertex position for linkage i, given with respect the fixed coordinate system O_{F}, is denoted by ${}^{\mathrm{F}}\mathbf{P}_i$. Therefore,

$$
\begin{aligned}
{}^{\mathrm{F}}\mathbf{P}_i &= \mathbf{D}^{\mathrm{F}}_{1,i}\ \mathbf{D}^{1,i}_{2,i}\ \mathbf{D}^{2,i}_{4,i} \begin{Bmatrix} 0 \\ 0 \\ 0 \\ 1 \end{Bmatrix} \\
&= \begin{Bmatrix} S\delta_{0,i} S\psi_{2,i}\ d_{2,i} + C\delta_{0,i}\ d \\ -C\delta_{0,i} S\psi_{2,i}\ d_{2,i} + S\delta_{0,i}\ d \\ C\theta_{1,i}(d_{1,i} + C\psi_{2,i}\ d_{2,i}) \\ 1 \end{Bmatrix}
\end{aligned} \tag{1}
$$

where,

$$
d = (d_{0,i} + S\theta_{1,i}\ d_{1,i} + C\psi_{2,i} S\theta_{1,i}\ d_{2,i}) \tag{2}
$$

and $\mathbf{D}^{\mathrm{F}}_{1,i}$, $\mathbf{D}^{1,i}_{2,i}$, and $\mathbf{D}^{2,i}_{4,i}$ are 4×4 homogeneous transformations given by

$$
\mathbf{D}^{\mathrm{F}}_{1,i} = \begin{bmatrix} C\delta_{0,i} & -S\delta_{0,i} & 0 & C\delta_{0,i}\ d_{0,i} \\ S\delta_{0,i} & C\delta_{0,i} & 0 & S\delta_{0,i}\ d_{0,i} \\ 0 & 0 & 1 & 0 \\ 0 & 0 & 0 & 1 \end{bmatrix} \tag{3}
$$

$$
\mathbf{D}^{1,i}_{2,i} = \begin{bmatrix} C\theta_{1,i} & 0 & S\theta_{1,i} & S\theta_{1,i}\ d_{1,i} \\ 0 & 1 & 0 & 0 \\ -S\theta_{1,i} & 0 & C\theta_{1,i} & C\theta_{1,i}\ d_{1,i} \\ 0 & 0 & 0 & 1 \end{bmatrix} \tag{4}
$$

and

$$
\mathbf{D}^{2,i}_{4,i} = \begin{bmatrix} 1 & 0 & 0 & 0 \\ 0 & C\psi_{2,i} & -S\psi_{2,i} & -S\psi_{2,i} d_{2,i} \\ 0 & S\psi_{2,i} & C\psi_{2,i} & C\psi_{2,i} d_{2,i} \\ 0 & 0 & 0 & 1 \end{bmatrix}. \tag{5}
$$

$\delta_{0,i}$ is a rotation about the z_{F} axis that aligns O_{F} with $O_{1,i}$ ($\delta_{0,1} = 0°$, $\delta_{0,2} = -120°$, $\delta_{0,3} = 120°$), and $d_{0,i}$ is the linear distance between the origins O_{F} and $O_{1,i}$. $\psi_{2,i}$ and $d_{2,i}$ are given by (see Figure 6)

$$
\psi_{2,i} = \frac{\pi}{2} - \frac{\theta_{2\mathrm{L},i} + \theta_{2\mathrm{R},i}}{2} \tag{6}
$$

and

$$
d_{2,i} = 2\ell \cos\left(\frac{\theta_{2\mathrm{L},i} - \theta_{2\mathrm{R},i}}{2}\right). \tag{7}
$$

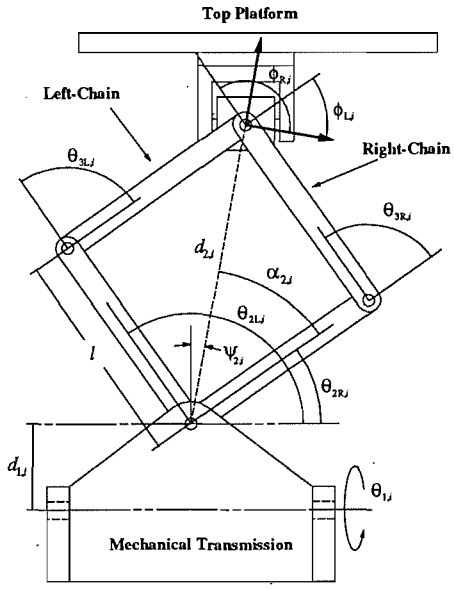

Figure 6: Parameters for Pantograph Linkage i.

The origin for the moving coordinate system, O_{M}, is at the top platform's centroid. Since the top platform is an equilateral triangle, the origin for O_{M} is at

$$^{\mathrm{F}}\mathbf{P}_{\mathrm{M}} = \frac{^{\mathrm{F}}\mathbf{P}_1 + ^{\mathrm{F}}\mathbf{P}_2 + ^{\mathrm{F}}\mathbf{P}_3}{3} \tag{8}$$

The orientation of the moving coordinate system O_{M} is denoted by the normal $^{\mathrm{F}}\mathbf{n}$, orientation $^{\mathrm{F}}\mathbf{o}$, and approach vectors $^{\mathrm{F}}\mathbf{a}$, which give directions for x_{M}, y_{M}, and z_{M}, respectively (see Paul [1981]). From Figure 7, we see that

$$^{\mathrm{F}}\mathbf{n} = \frac{(^{\mathrm{F}}\mathbf{P}_1 - ^{\mathrm{F}}\mathbf{P}_2) + 1/2(^{\mathrm{F}}\mathbf{P}_2 - ^{\mathrm{F}}\mathbf{P}_3)}{|(^{\mathrm{F}}\mathbf{P}_1 - ^{\mathrm{F}}\mathbf{P}_2) + 1/2(^{\mathrm{F}}\mathbf{P}_2 - ^{\mathrm{F}}\mathbf{P}_3)|} \tag{9}$$

$$^{\mathrm{F}}\mathbf{o} = \frac{^{\mathrm{F}}\mathbf{P}_3 - ^{\mathrm{F}}\mathbf{P}_2}{|^{\mathrm{F}}\mathbf{P}_3 - ^{\mathrm{F}}\mathbf{P}_2|} \tag{10}$$

$$^{\mathrm{F}}\mathbf{a} = ^{\mathrm{F}}\mathbf{n} \times ^{\mathrm{F}}\mathbf{o} \tag{11}$$

The forward kinematics for this device is completely specified by $^{\mathrm{F}}\mathbf{n}$, $^{\mathrm{F}}\mathbf{o}$, $^{\mathrm{F}}\mathbf{a}$, and $^{\mathrm{F}}\mathbf{P}_{\mathrm{M}}$, which form the 4×4 coordinate transformation

$$\mathbf{D}^{\mathrm{F}}_{\mathrm{M}} = \begin{bmatrix} ^{\mathrm{F}}n_x & ^{\mathrm{F}}o_x & ^{\mathrm{F}}a_x & ^{\mathrm{F}}P_x \\ ^{\mathrm{F}}n_y & ^{\mathrm{F}}o_y & ^{\mathrm{F}}a_y & ^{\mathrm{F}}P_y \\ ^{\mathrm{F}}n_z & ^{\mathrm{F}}o_z & ^{\mathrm{F}}a_z & ^{\mathrm{F}}P_z \\ 0 & 0 & 0 & 1 \end{bmatrix}. \tag{12}$$

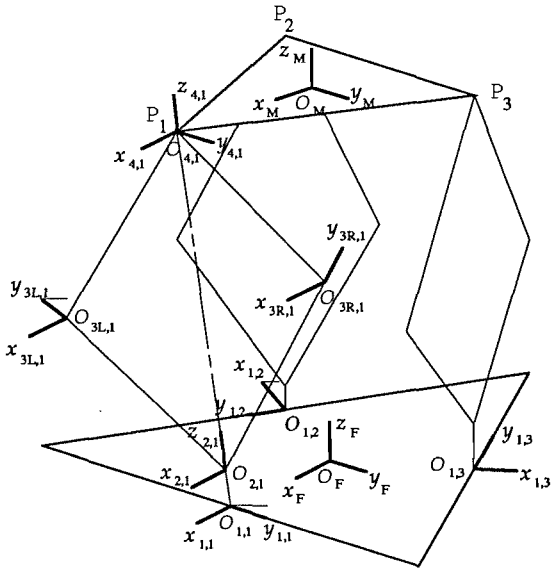

Figure 7: Generalized Controller Kinematic Skeleton

5.2 Top Platform Twist

The top platform's Cartesian velocity, relative to the base platform, is necessary for bilateral control of a remote slave manipulator. The actuator rates $\dot{\theta}_{2\mathrm{L},i}$ and $\dot{\theta}_{2\mathrm{R},i}$ are known, as they are computed from encoders located on the motor shafts. However, the top platform twist, $\bar{\mathbf{T}} = \{\, \omega_x, \omega_y, \omega_z;\ v_x, v_y, v_z \,\}^{\mathrm{T}}$ is unknown.

Since the generalized master controller is a hybrid serial/parallel mechanism, with both passive and active joints, the method outlined by Kumar [1992] offers a straight-forward procedure for obtaining $\bar{\mathbf{T}}$ — this procedure does not require encoder measurements of passive actuators (see also Mohamed and Duffy [1985]).

For each left sub-chain, the top platform twist $\bar{\mathbf{T}}$ is a linear combination of the actuator-screws

$$\bar{\mathbf{T}} = \dot{\theta}_{1,i}\ \bar{\mathbf{S}}_{1,i} + \dot{\theta}_{2\mathrm{L},i}\ \bar{\mathbf{S}}_{2\mathrm{L},i} + \dot{\theta}_{3\mathrm{L},i}\ \bar{\mathbf{S}}_{3\mathrm{L},i} + \dot{\theta}_{\mathrm{S},i}\ \bar{\mathbf{S}}_{\mathrm{S},i} \tag{13}$$

where, $\dot{\theta}_{1,i}$, $\dot{\theta}_{2\mathrm{L},i}$, and $\dot{\theta}_{3\mathrm{L},i}$ are actuator rates and $\dot{\theta}_{\mathrm{S},i}\ \bar{\mathbf{S}}_{\mathrm{S},i}$ is a twist about the spherical three-system located at the ball-in-socket joint. The rates of the passive joints $\dot{\theta}_{1,i}$, $\dot{\theta}_{3\mathrm{L},i}$, and $\dot{\theta}_{\mathrm{S},i}$ are eliminated from Equation (13) by using the concept of reciprocity.

The virtual product, $\varpi_{1,2}$, between two screws $\bar{\mathbf{S}}_1$ and $\bar{\mathbf{S}}_2$, whose coordinates are given by (see Roth [1984])

$$\bar{\mathbf{S}}_1 = \left\{ \begin{array}{c} \mathbf{s}_1 \\ \mathbf{s}_{o1} \end{array} \right\}_{6\times 1} \qquad \bar{\mathbf{S}}_2 = \left\{ \begin{array}{c} \mathbf{s}_2 \\ \mathbf{s}_{o2} \end{array} \right\}_{6\times 1}$$

is defined as

$$\varpi_{1,2} = [\Pi\ \bar{\mathbf{S}}_1]^{\mathrm{T}}\ \bar{\mathbf{S}}_2 = [\Pi\ \bar{\mathbf{S}}_2]^{\mathrm{T}}\ \bar{\mathbf{S}}_1 \tag{14}$$

where, the operator Π transforms screw coordinates from ray (axis) coordinates to axis (ray) coordinates and is given by

$$\Pi = \begin{bmatrix} \mathbf{0}_3 & \mathbf{I}_3 \\ \mathbf{I}_3 & \mathbf{0}_3 \end{bmatrix} \tag{15}$$

and, $\mathbf{I}_3$ and $\mathbf{0}_3$ are the 3×3 identity and zero matrices, respectively. The operator Π has the following properties:

$$\Pi^{\mathrm{T}} = \Pi \quad \text{and} \quad \Pi^{-1} = \Pi$$

Two screws $\bar{\mathbf{S}}_1$ and $\bar{\mathbf{S}}_2$ are reciprocal when the virtual product, as defined by Equation (14), is zero (see Ball [1900]).

Let $\bar{\mathbf{S}}'_{2\mathrm{L},i}$ be the screw reciprocal to $\bar{\mathbf{S}}_{1,i}$, $\bar{\mathbf{S}}_{3\mathrm{L},i}$, and $\bar{\mathbf{S}}_{\mathrm{S},i}$ excluding $\bar{\mathbf{S}}_{2\mathrm{L},i}$. In general $\bar{\mathbf{S}}_{1,i}$, $\bar{\mathbf{S}}_{3\mathrm{L},i}$, and $\bar{\mathbf{S}}_{\mathrm{S},i}$ will form a five-system and $\bar{\mathbf{S}}'_{2\mathrm{L},i}$ is unique. Taking the virtual product of $\bar{\mathbf{S}}'_{2\mathrm{L},i}$ with Equation (13) and solving for $\dot{\theta}_{2\mathrm{L},i}$ we obtain

$$\dot{\theta}_{2\mathrm{L},i} = \frac{[\Pi\, \bar{\mathbf{S}}'_{2\mathrm{L},i}]^{\mathrm{T}}\, \bar{\mathbf{T}}}{[\Pi\, \bar{\mathbf{S}}'_{2\mathrm{L},i}]^{\mathrm{T}}\, \bar{\mathbf{S}}_{2\mathrm{L},i}}. \tag{16}$$

$\bar{\mathbf{S}}'_{2\mathrm{L},i}$ is obtained by first noting that all screws reciprocal the spherical three-system are zero-pitch and intersect the O_4 coordinate system. In the O_4 coordinate system, $\bar{\mathbf{S}}'_{2\mathrm{L},i}$ is given by

$${}^4\bar{\mathbf{S}}'_{2\mathrm{L},i} = \{\, s'_{2\mathrm{L},ix}, s'_{2\mathrm{L},iy}, s'_{2\mathrm{L},iz}; 0, 0, 0 \,\}^{\mathrm{T}} \tag{17}$$

$s'_{2\mathrm{L},ix}$, $s'_{2\mathrm{L},iy}$, and $s'_{2\mathrm{L},iz}$ can be obtained with the following conditions

$$[\Pi\, \bar{\mathbf{S}}'_{2\mathrm{L},i}]^{\mathrm{T}}\, \bar{\mathbf{S}}_{1,i} = 0 \quad \underline{\text{RECIPROCITY}}$$

$$[\Pi\, \bar{\mathbf{S}}'_{2\mathrm{L},i}]^{\mathrm{T}}\, \bar{\mathbf{S}}_{3\mathrm{L},i} = 0 \quad \underline{\text{RECIPROCITY}}$$

$$|\bar{\mathbf{S}}'_{2\mathrm{L},i}| = 1 \quad \underline{\text{UNIT MAGNITUDE}}$$

Thus,

$${}^4\bar{\mathbf{S}}'_{2\mathrm{L},i} = \{\, 0, \pm\cos\phi_L, \pm\sin\phi_L; 0, 0, 0 \,\}^{\mathrm{T}} \tag{18}$$

where,

$$\phi_{\mathrm{L}} = \frac{\pi}{2} - \frac{\theta_{2\mathrm{L},i} - \theta_{2\mathrm{R},i}}{2}. \tag{19}$$

Similarly, for each right sub-chain we have

$$\dot{\theta}_{2\mathrm{R},i} = \frac{[\Pi\, \bar{\mathbf{S}}'_{2\mathrm{R},i}]^{\mathrm{T}}\, \bar{\mathbf{T}}}{[\Pi\, \bar{\mathbf{S}}'_{2\mathrm{R},i}]^{\mathrm{T}}\, \bar{\mathbf{S}}_{2\mathrm{R},i}} \tag{20}$$

and

$${}^4\bar{\mathbf{S}}'_{2\mathrm{R},i} = \{\, 0, \pm\cos\phi_R, \pm\sin\phi_R; 0, 0, 0 \,\}^{\mathrm{T}} \tag{21}$$

where,

$$\phi_{\mathrm{R}} = \frac{\pi}{2} + \frac{\theta_{2\mathrm{L},i} - \theta_{2\mathrm{R},i}}{2}. \tag{22}$$

The denominators in Equations (16) and (20) are given by

$$[\Pi \bar{\mathbf{S}}'_{2\mathrm{L},i}]^{\mathrm{T}}\, \bar{\mathbf{S}}_{2\mathrm{L},i} = -\ell \sin\left(\theta_{2\mathrm{L},i} - \theta_{2\mathrm{R},i}\right) \tag{23}$$

and

$$[\Pi \bar{\mathbf{S}}'_{2\mathrm{R},i}]^{\mathrm{T}}\, \bar{\mathbf{S}}_{2\mathrm{R},i} = \ell \sin\left(\theta_{2\mathrm{L},i} - \theta_{2\mathrm{R},i}\right) \tag{24}$$

Amalgamating the expressions for $\dot{\theta}_{2\mathrm{L},i}$ and $\dot{\theta}_{2\mathrm{R},i}$ $(i = 1, 2, 3)$ into a single transformation, we obtain

$$\dot{\boldsymbol{\Theta}} = \boldsymbol{\Gamma}^{\mathrm{T}}\, \bar{\mathbf{T}} \tag{25}$$

where, $\dot{\boldsymbol{\Theta}} = \{\dot{\theta}_{2\mathrm{L},1}, \dot{\theta}_{2\mathrm{R},1}, \dot{\theta}_{2\mathrm{L},2}, \dot{\theta}_{2\mathrm{R},2}, \dot{\theta}_{2\mathrm{L},3}, \dot{\theta}_{2\mathrm{R},3}\}^{\mathrm{T}}$ and $\boldsymbol{\Gamma}$ is a 6×6 "Jacobian." For the actuation pair $\{\dot{\theta}_{2\mathrm{L},i}, \dot{\theta}_{2\mathrm{R},i}\}$, the columns of $\boldsymbol{\Gamma}$ are given by

$$\left[\begin{array}{cc} \dfrac{[\Pi \bar{\mathbf{S}}'_{2\mathrm{L},i}]}{[\Pi \bar{\mathbf{S}}'_{2\mathrm{L},i}]^{\mathrm{T}}\, \bar{\mathbf{S}}_{2\mathrm{L},i}} & \dfrac{[\Pi \bar{\mathbf{S}}'_{2\mathrm{R},i}]}{[\Pi \bar{\mathbf{S}}'_{2\mathrm{R},i}]^{\mathrm{T}}\, \bar{\mathbf{S}}_{2\mathrm{R},i}} \end{array}\right] \tag{26}$$

If $\boldsymbol{\Gamma}$ is nonsingular, then Equation (25) can be inverted to obtain the top platform twist

$$\bar{\mathbf{T}} = [\boldsymbol{\Gamma}^{-1}]^{\mathrm{T}}\, \dot{\boldsymbol{\Theta}} \tag{27}$$

The singularities of $\boldsymbol{\Gamma}$ occur when

$$C\theta_{1,i} = 0 \;\rightarrow\; \theta_{1,i} = \pm\frac{\pi}{2} \tag{28}$$

$$\sin(\theta_{2\mathrm{L},i} - \theta_{2\mathrm{R},i}) = 0 \;\rightarrow\; \begin{array}{l} \theta_{2\mathrm{L},i} - \theta_{2\mathrm{R},i} = 0 \\ \theta_{2\mathrm{L},i} - \theta_{2\mathrm{R},i} = \pm\pi \\ \text{for} \quad i = 1, 2, 3 \end{array} \tag{29}$$

5.3 Force-Reflection

We are investigating the implementation of several control algorithms for the master/slave manipulation system. Our primary concern, however, is the reflection of slave end-effector forces to the generalized hand controller. The proceeding force-reflection scheme closely follows the active stiffness control formulation originally given by Salisbury [1980, 1982] — the geometrical insights provided by Patterson and Lipkin [1990a, 1990b] and Griffis and Duffy [1991] are also considered.

When the top platform is displaced from a nominal Cartesian position

$$\mathbf{X}_o = \{x_o, y_o, z_o; \phi_{x,o}, \phi_{y,o}, \phi_{z,o}\}^{\mathrm{T}}, \tag{30}$$

its reaction forces and resulting motion should emulate a rigid-body attached to a six-dimensional spring. The top platform's restoring wrenches are provided by torques on the master controller actuator-screw system.

The stiffness formulation given by Salisbury requires the reaction wrench to be proportional to the displacement from the nominal position

$$\bar{\mathbf{W}}_M = \mathbf{K}_M \, d\mathbf{X} \tag{31}$$

where, $\mathbf{K}_M$ is a 6×6 stiffness matrix, $d\mathbf{X}$ is the differential displacement from the nominal position, and the reaction wrench on the master controller is comprised of a force $\mathbf{f}$ and moment $\mathbf{m}$ ($\bar{\mathbf{W}} = \{ f_x, f_y, f_z; m_x, m_y, m_z \}^{\mathrm{T}}$).

The top platform twist $\bar{\mathbf{T}}$ is related to the differential Cartesian displacement $d\mathbf{X}$ and actuator displacements $d\Theta$ by

$$\Pi \, d\mathbf{X} = \bar{\mathbf{T}} \, dt = [\mathbf{\Gamma}^{-1}]^{\mathrm{T}} \, d\Theta \tag{32}$$

Thus, Equation (31) becomes

$$\bar{\mathbf{W}}_M = \mathbf{K}_M \, \Pi [\mathbf{\Gamma}^{-1}]^{\mathrm{T}} \, d\Theta \tag{33}$$

From Kumar [1992], the top platform wrench $\bar{\mathbf{W}}_M$ is given by

$$\bar{\mathbf{W}}_M = \Pi \, \mathbf{\Gamma} \, \mathcal{T} \tag{34}$$

where, $\mathcal{T} = \{\tau_{2\mathrm{L},1}, \tau_{2\mathrm{R},1}, \tau_{2\mathrm{L},2}, \tau_{2\mathrm{R},2}, \tau_{2\mathrm{L},3}, \tau_{2\mathrm{R},3}\}^{\mathrm{T}}$ is a 6×1 vector of actuator torques. Therefore, from Equations (33) and (34), we obtain

$$\mathcal{T} = \mathbf{K}_{\theta M} \, d\Theta \tag{35}$$

where, the actuator stiffness matrix $\mathbf{K}_{\theta M}$ is given by

$$\mathbf{K}_{\theta M} = \left[\mathbf{\Gamma}^{-1}\right] \, \Pi \, \mathbf{K}_M \, \Pi \left[\mathbf{\Gamma}^{-1}\right]^{\mathrm{T}} \tag{36}$$

A wrist force/torque sensor is used to measure the reaction wrenches at the slave manipulator/environment interface. The reaction wrench system at the manipulator/environment interface is resolved into orthogonal components of force and moment. Using this approach, the wrench system is then superimposed on the top platform as bias forces.

The wrench system on the slave manipulator's end-effector is resolved in a Cartesian coordinate system $O_{F'}$ parallel to the master controller base coordinate system O_F. These forces are then scaled by a factor σ that correlates with the operator's maximum fatigue strength. Therefore, after taking into account the bias forces, the commanded actuator torques become

$$\mathcal{T} = \mathbf{K}_{\theta M} \, d\Theta + \sigma [\mathbf{\Gamma}^{-1}] \, \Pi \, {}^{F'}\bar{\mathbf{W}}_S \tag{37}$$

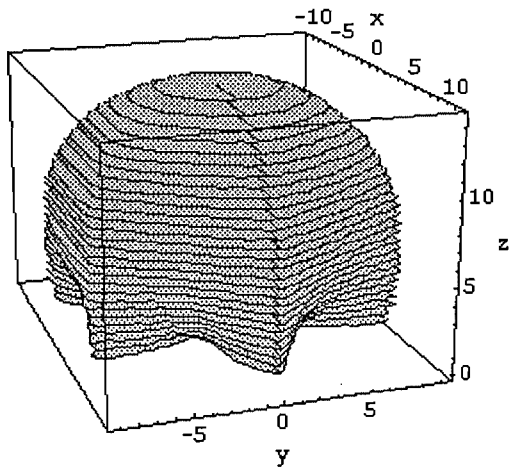

Figure 8: Top Platform Center-Point Workspace

5.4 Workspace

The master hand controller's workspace characteristics will partially determine the effectiveness of remote slave manipulation. Figure 8 displays a 3-dimensional volume representation of reachable points for the top platform center, when the top platform's orientation is parallel to the base. The reachable workspace was determined numerically with an inverse kinematics search algorithm.

For a symmetrical arrangement of link lengths ℓ, equilateral base and top platforms, the workspace shape and volume is strictly determined by $d_{0,i}$ (or $d_{M,i}$) and the ratio $d_{M,i}/d_{0,i}$ — $d_{M,i}$ is the linear distance between the origins O_{M} and $O_{4,i}$ (in Figure 8 the ratio $d_{M,i}/d_{0,i} = 1.0$). For the illustration in Figure 8, horizontal cross-sections near the upper workspace region are circular, while horizontal cross-sections near the base plane form 6 point stars.

Changing the ratio $d_{M,i}/d_{0,i}$ affects the total volume and shape. For ratios $d_{M,i}/d_{0,i} = 1.5$ and $d_{M,i}/d_{0,i} = 0.5$, the workspaces' horizontal cross-sectional shapes become distorted and less circular near the base and upper regions. The shapes and volumes for these two workspaces are identical with tops and bases inverted, and the total volume decreases five percent from the case $d_{M,i}/d_{0,i} = 1.0$. A discussion on optimum link sizes ℓ and optimum ratio $d_{M,i}/d_{0,i}$ will be summarized at a later date.

6 Discussion and Extensions

The generalized telerobotic controller project was a fruitful learning experience. In this endeavor, we demonstrated several successful design concepts as well as illustrated useful theory on screw systems. Among the design concepts were the hybrid series/parallel struc-

ture, a spherical joint design, new cable termination and pre-tensioning techniques, and an inertially stable drive system. The practical use of reciprocal screw systems to determine the top platform twist was also enlightening. Through this design process we have enhanced our understanding and are now poised for several design improvements.

Some component improvements include: top platform size, spherical joint attachment, split pulley accessibility, single stage transmission design, pantograph link joint bearings, motor/split pulley coupling, wire routing, repeatable home position, and reconfiguration of motor placement for better accessibility. New motor and encoder selections as well as bearings will significantly improve overall controller flexibility and performance.

These suggestions can be incorporated into a second prototype with particular attention given to performance, safety, modularity, and manufacturability. A second prototype would be professionally machined and manufactured to exact specifications. Furthermore, there several preliminary theoretical investigations should be done before a second prototype design is finalized. These investigations require studying the effects of various enhancements controller functionality.

7 Bibliography

[1] Robert S. Ball. *A Treatise on the Theory of Screws.* The University Press, Cambridge, England, 1900.

[2] Patrick Fischer, Ron Daniel, and K. V. Siva. Specification and design of input devices for teleoperation. In *Proceedings, 1990 IEEE International Conference on Robotics and Automation*, pages 540–545, 1990.

[3] M. Griffis and J. Duffy. Kinestatic control: A novel theory for simultaneously regulating force and displacement. *ASME Journal of Mechanical Design*, 113:508–515, 1991.

[4] Hirochika Inoue, Yuji Tsusaka, and Takeshi Fukuizumi. Parallel manipulator. In O.D. Fuageras and G. Giralt, editors, *Robotics Research: The Third International Symposium*, pages 321–327. MIT Press, Cambridge, Massachusetts, 1986.

[5] V. Kumar. Instantaneous kinematics of parallel-chain robotic mechanisms. *ASME Journal of Mechanical Design*, 114(3):349–358, 1992.

[6] Gregory L. Long and Curtis L. Collins. A pantograph linkage parallel platform master hand controller for force-reflection. In *Proceedings, 1992 IEEE International Conference on Robotics and Automation*, pages 390–395, 1992.

[7] M. G. Mohamed and J. Duffy. A direct determination of the instantaneous kinematics of fully parallel robot manipulators. *Transactions of the ASME: Journal of Mechanisms, Transmissions, and Automation in Design*, 107:226–229, June 1985.

[8] Timothy Patterson and Harvey Lipkin. A classification of robot compliance. In *Proceedings 21st ASME Mechanisms Conference*, pages 307–314, 1990.

[9] Richard P. Paul. *Robot Manipulators: Mathematics, Programming, and Control.* The MIT Press, Cambridge, Massachusetts, 1981.

[10] Bernard Roth. Screws, motors, and wrenches that cannot be bought in a hardware store. *Robotics Research: The First International Symposium*, pages 679–693, 1984.

[11] J. Kenneth Salisbury. Active stiffness control of a manipulator in cartesian coordinates. In *Proceedings of the 1980 IEEE Decision and Control Conference*, 1980.

[12] J. Kenneth Salisbury and John J. Craig. Articulated hands: Force control and kinematic issues. *The International Journal of Robotics Research*, 1(1):4–17, 1982.

[13] Kenneth Salisbury. Whole arm manipulation. *Robotics Research: The Fourth International Symposium*, pages 183–189, 1987.

[14] William T. Townsend. *The Effect of Transmission Design on Force-Controlled Manipulator Performance.* PhD thesis, Massachusetts Institute of Technology, 1988.

A Mechanical Drawings

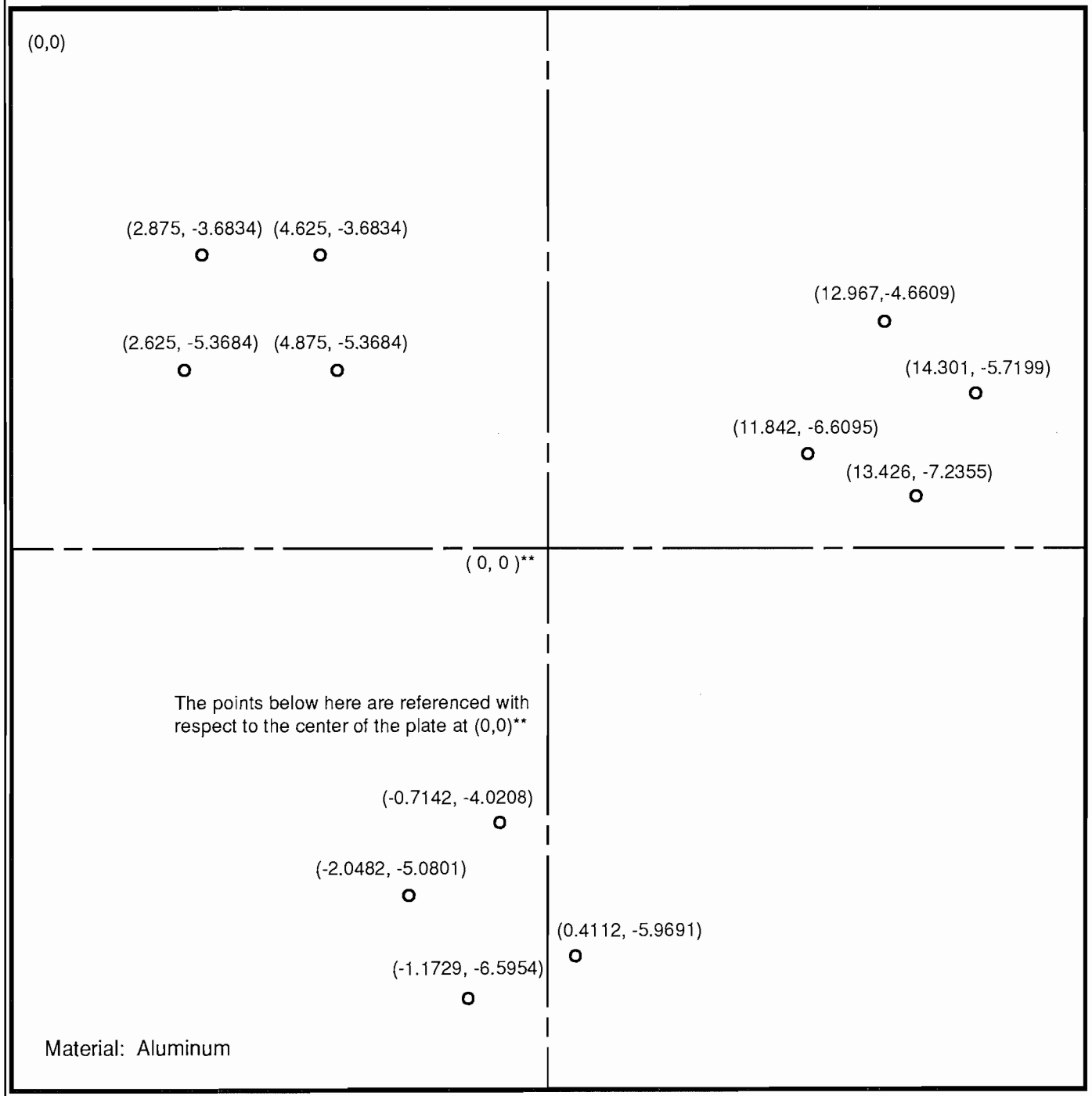

This is the hole layout for the base plate. It is prepared for direct referencing on the mill. All holes are 0.161.

Countersink for flathead screws

This piece is made from 1/4 plate milled to a 16" square

University of California, Irvine Department of Mechanical and Aerospace Engineering Robotics Lab, ELF 131 (714) 856-8051	
Base Plate	
DRAWN C. Collins	DWG NO. None
DATE 3/93	SCALE –

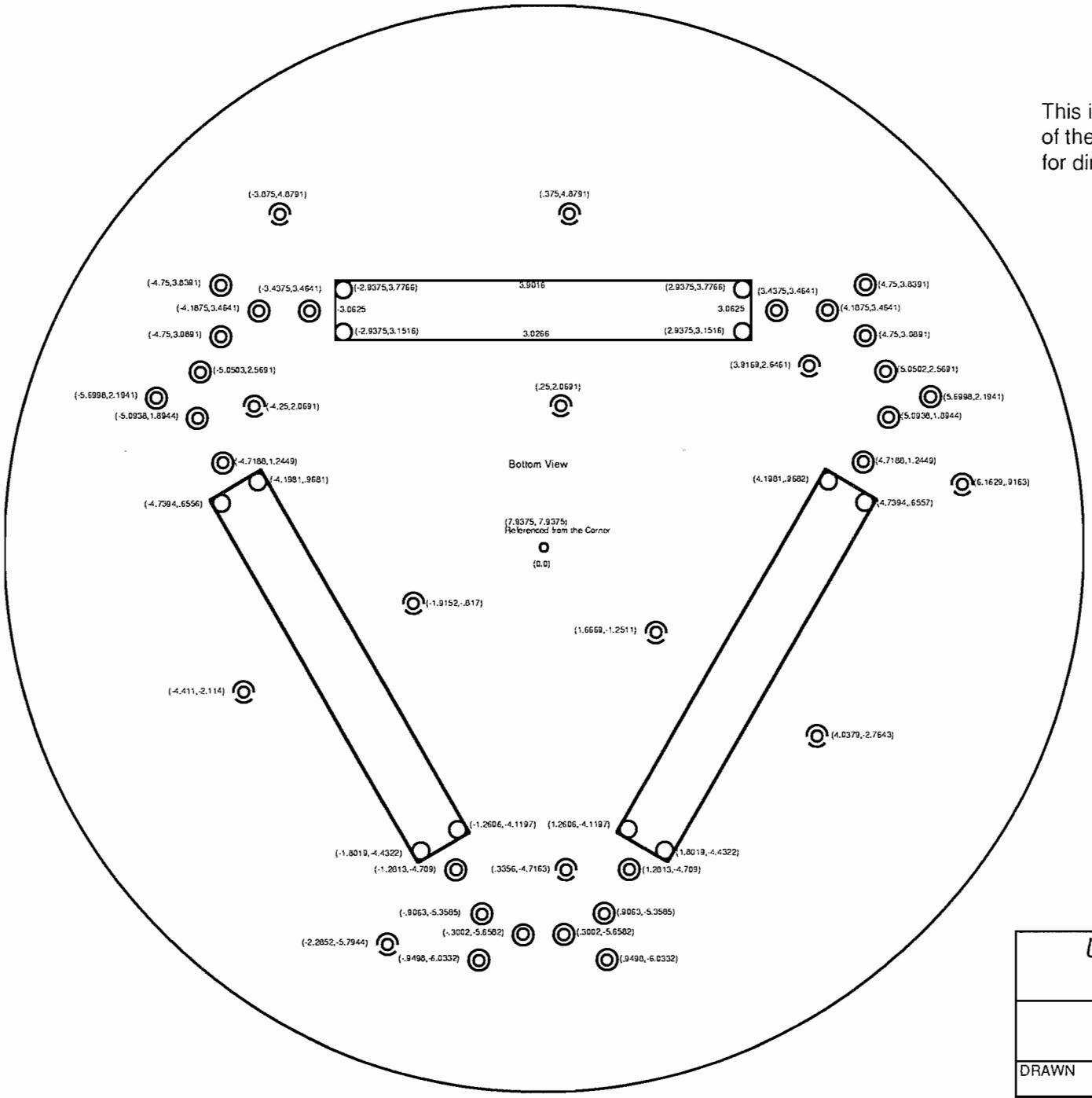

This is a layout for the hole and slot pattern of the base platform prepared for direct referencing on the mill

This piece is made from 1/4 plate milled to a 16" circle.

University of California, Irvine Department of Mechanical and Aerospace Engineering Robotics Lab, ELF 131 (714) 856-8051	
Base Platform	
DRAWN C. Collins	DWG NO. None
DATE 3/93	SCALE –

Material: Aluminum

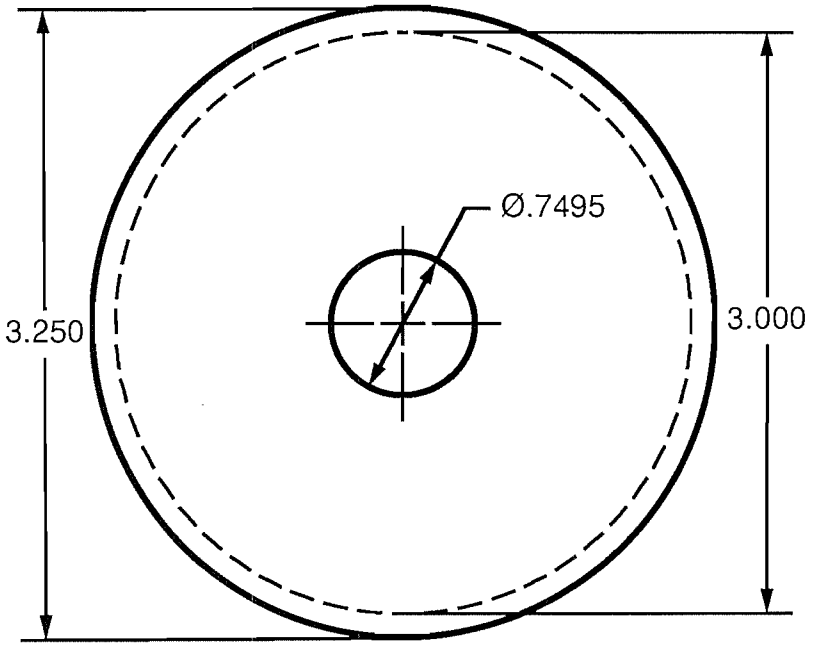

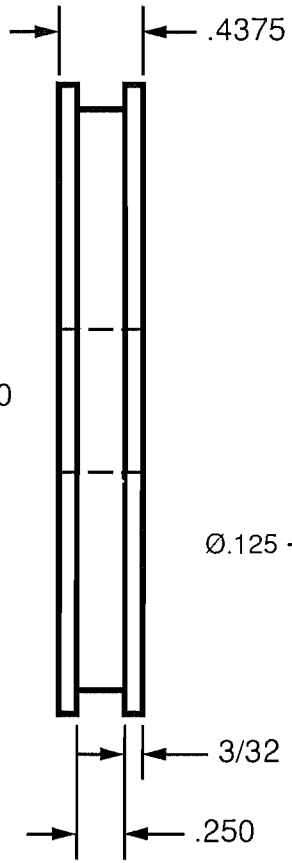

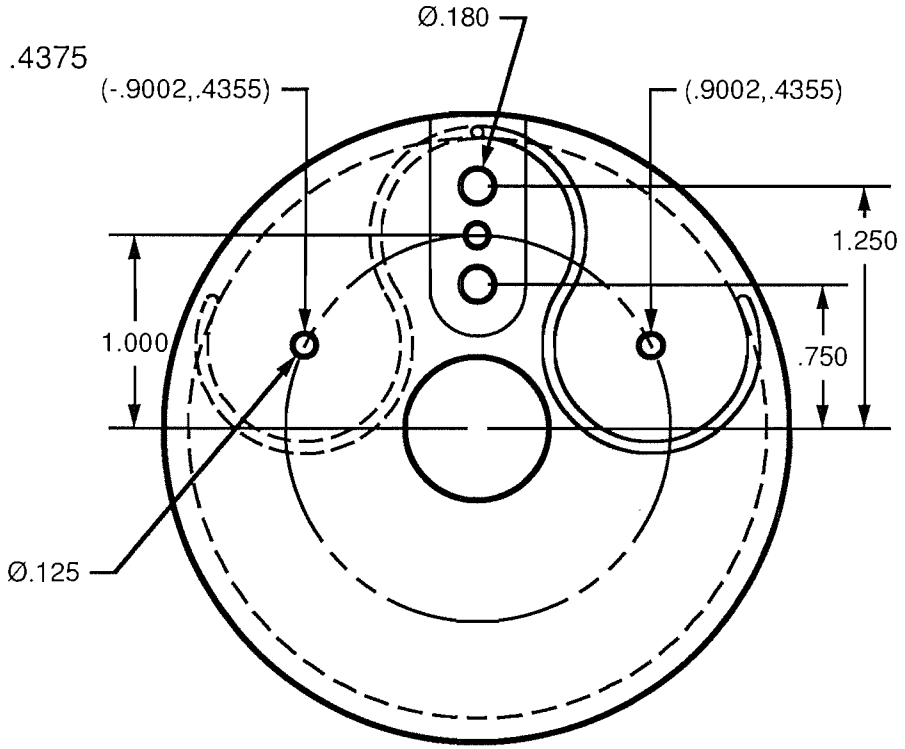

Groove Detail

Mill grooves 1/16 wide, 0.1 deep.

Material: Aluminum

University of California, Irvine
Department of Mechanical and Aerospace Engineering
Robotics Lab, ELF 131 (714) 856-8051

Driven Pulley

DRAWN	C. Collins	QUANTITY	6
DATE	3/93	SCALE	FULL

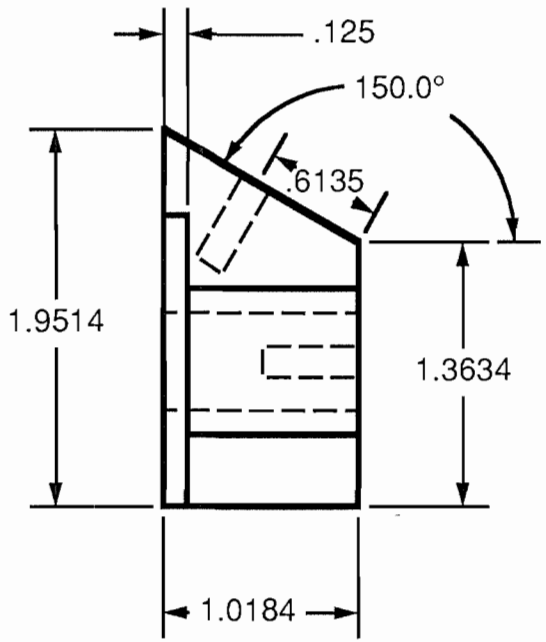

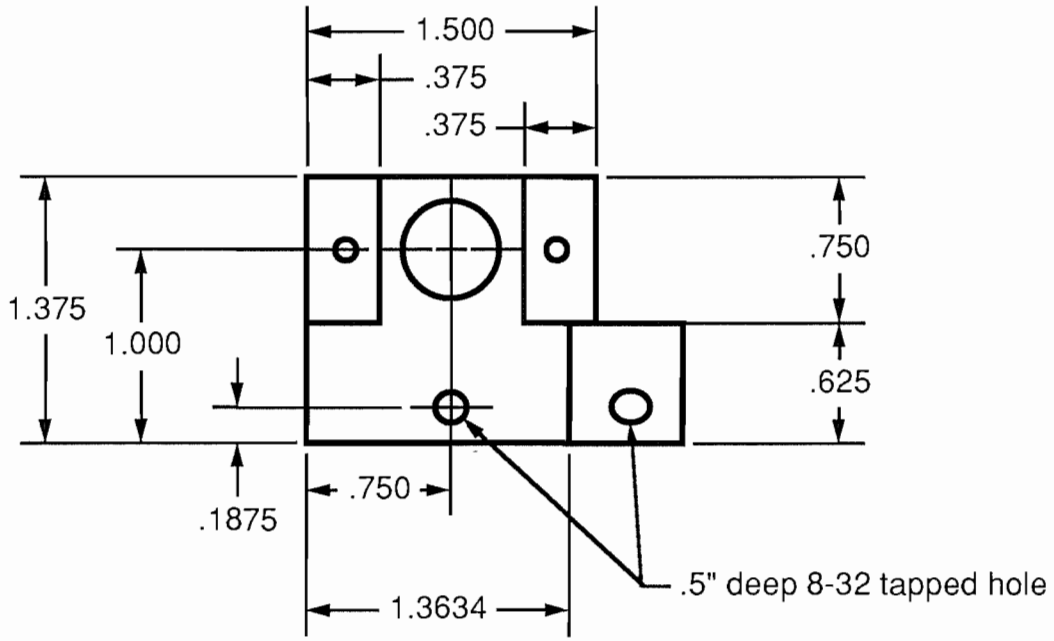

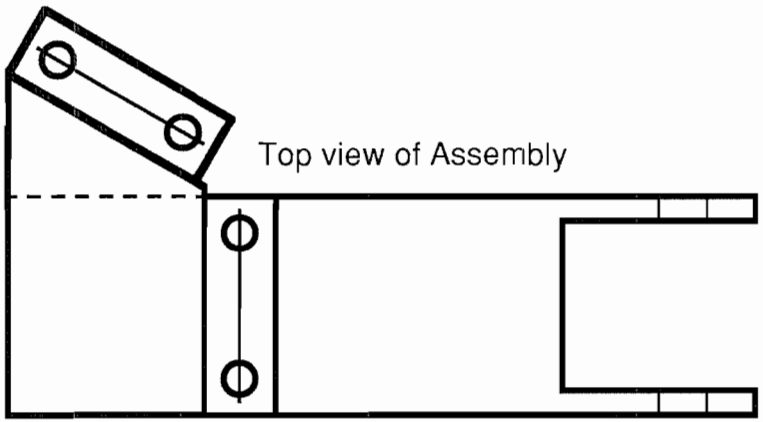

Material: Aluminum

University of California, Irvine
Department of Mechanical and Aerospace Engineering
Robotics Lab, ELF 131 (714) 856-8051

Encoder Mounts

DRAWN	C. Collins	QUANTITY	3
DATE	3/93	SCALE	FULL

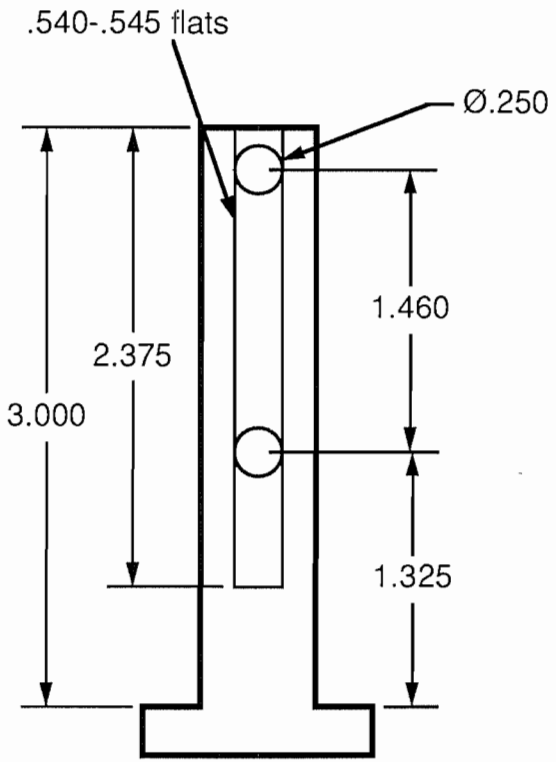

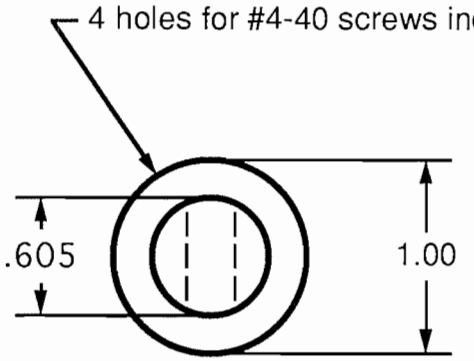

Modify dimensions and screw holes as needed to fit plastic video game joystick handle.

Material: Aluminum

University of California, Irvine
Department of Mechanical and Aerospace Engineering
Robotics Lab, ELF 131 (714) 856-8051

Hand Gripper Support

DRAWN	C. Collins	QUANTITY	1
DATE	3/93	SCALE	FULL

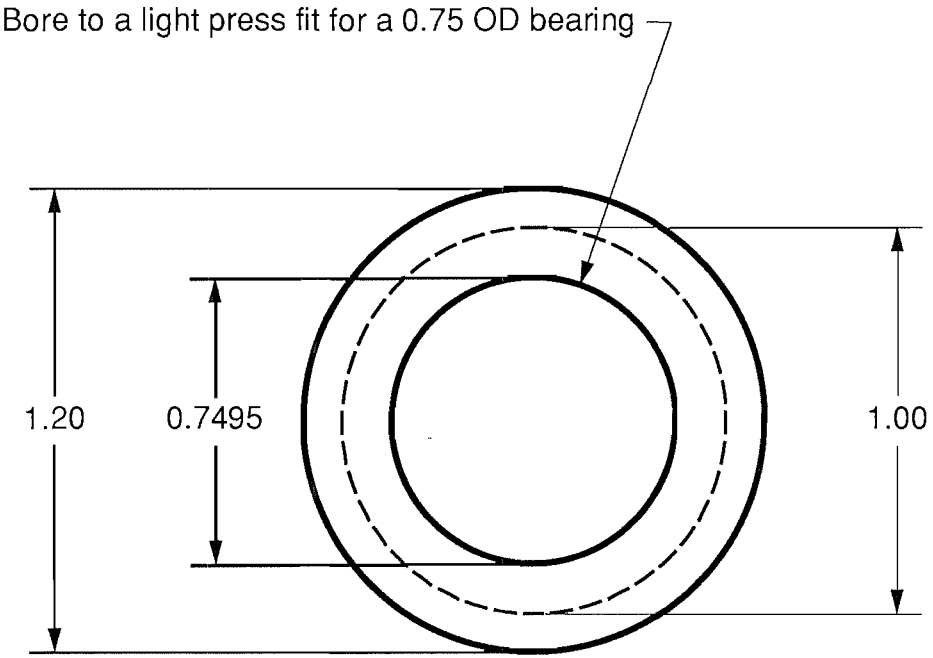

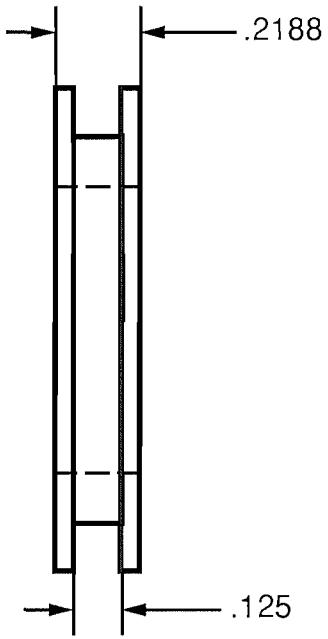

University of California, Irvine	
Department of Mechanical and Aerospace Engineering Robotics Lab, ELF 131 (714) 856-8051	
Idler Pulley	
DRAWN C. Collins	QUANTITY 12
DATE 3/93	SCALE 2:1

Material: Aluminum

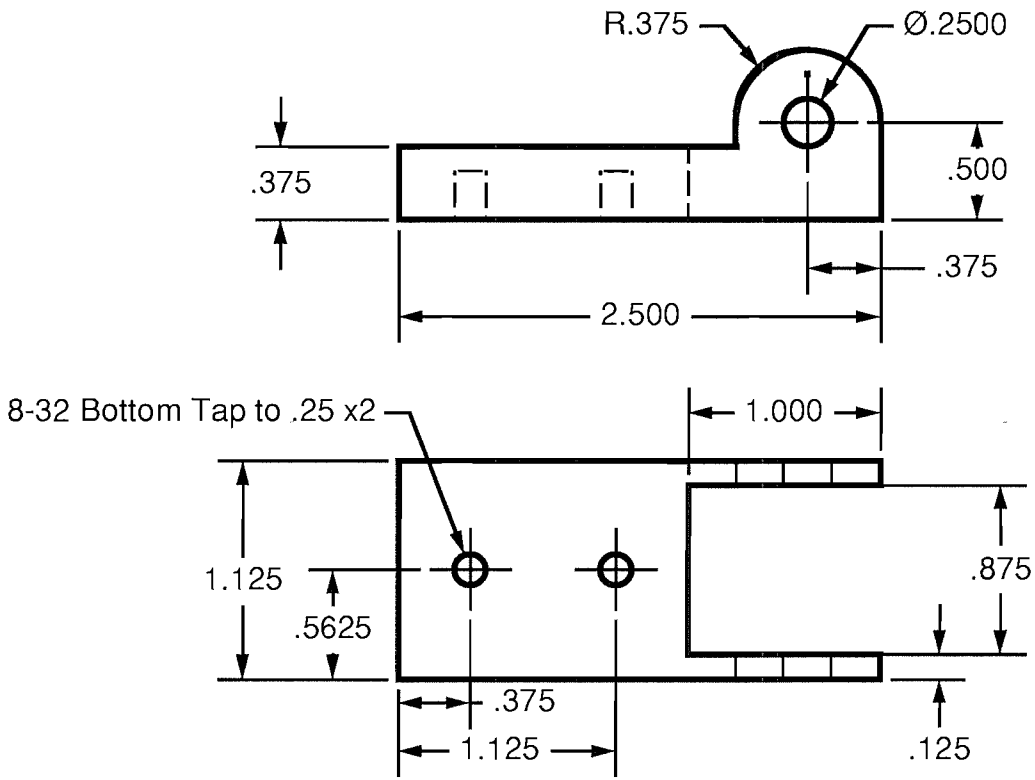

Bottom View

University of California, Irvine
Department of Mechanical and Aerospace Engineering
Robotics Lab, ELF 131 (714) 856-8051

Idler Pulley Support

DRAWN	C. Collins	QUANTITY	6
DATE	3/93	SCALE	FULL

Material: Aluminum

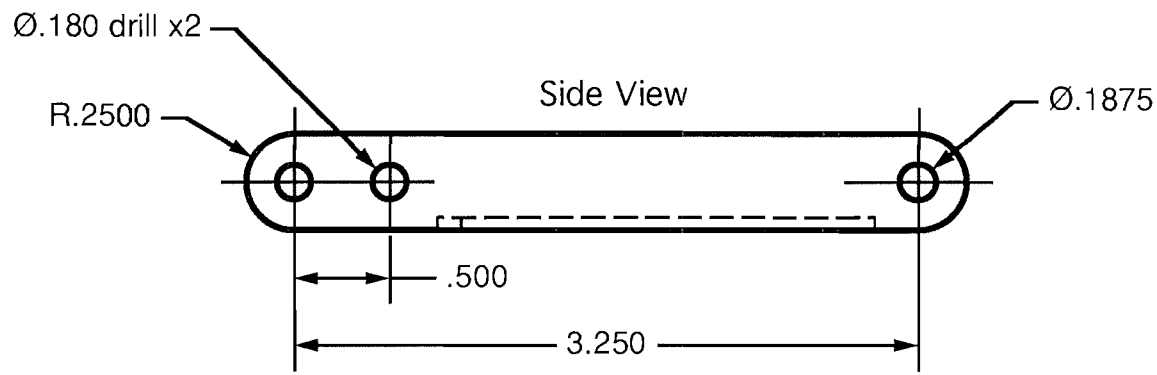

Use Standard Channeling

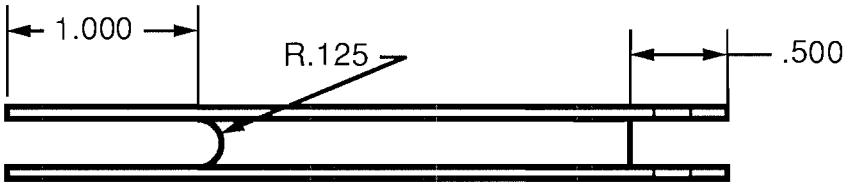

Top view

Material: Aluminum

University of California, Irvine
Department of Mechanical and Aerospace Engineering
Robotics Lab, ELF 131 (714) 856-8051

Lower Pantograph Link

DRAWN	C. Collins	QUANTITY	6
DATE	3/93	SCALE	FULL

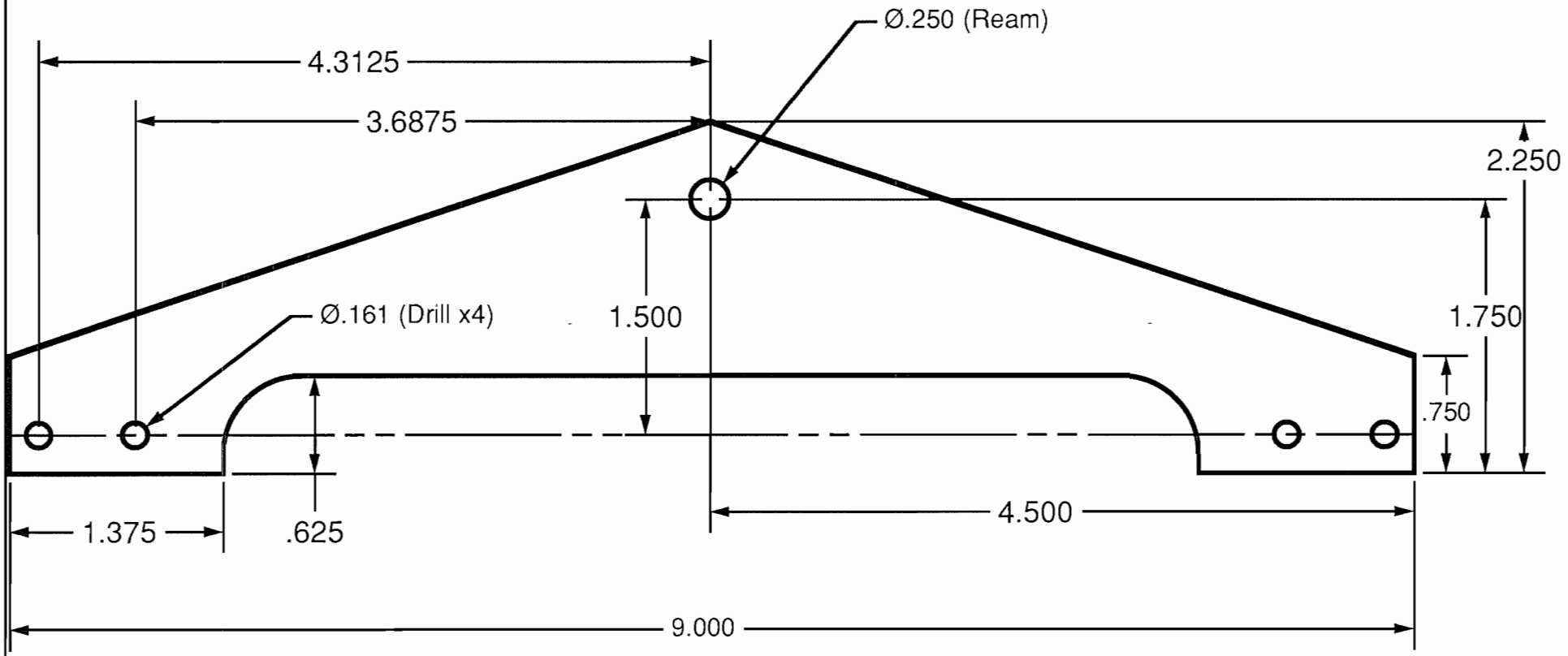

Piece to be machined from 1/8" sheet metal
Finish: Sand Blast

University of California, Irvine Department of Mechanical and Aerospace Engineering Robotics Lab, ELF 131 (714) 856-8051	
Pantograph Housing Plate	
DRAWN C. Collins	QUANTITY 6
DATE 3/93	SCALE FULL

Material: Aluminum

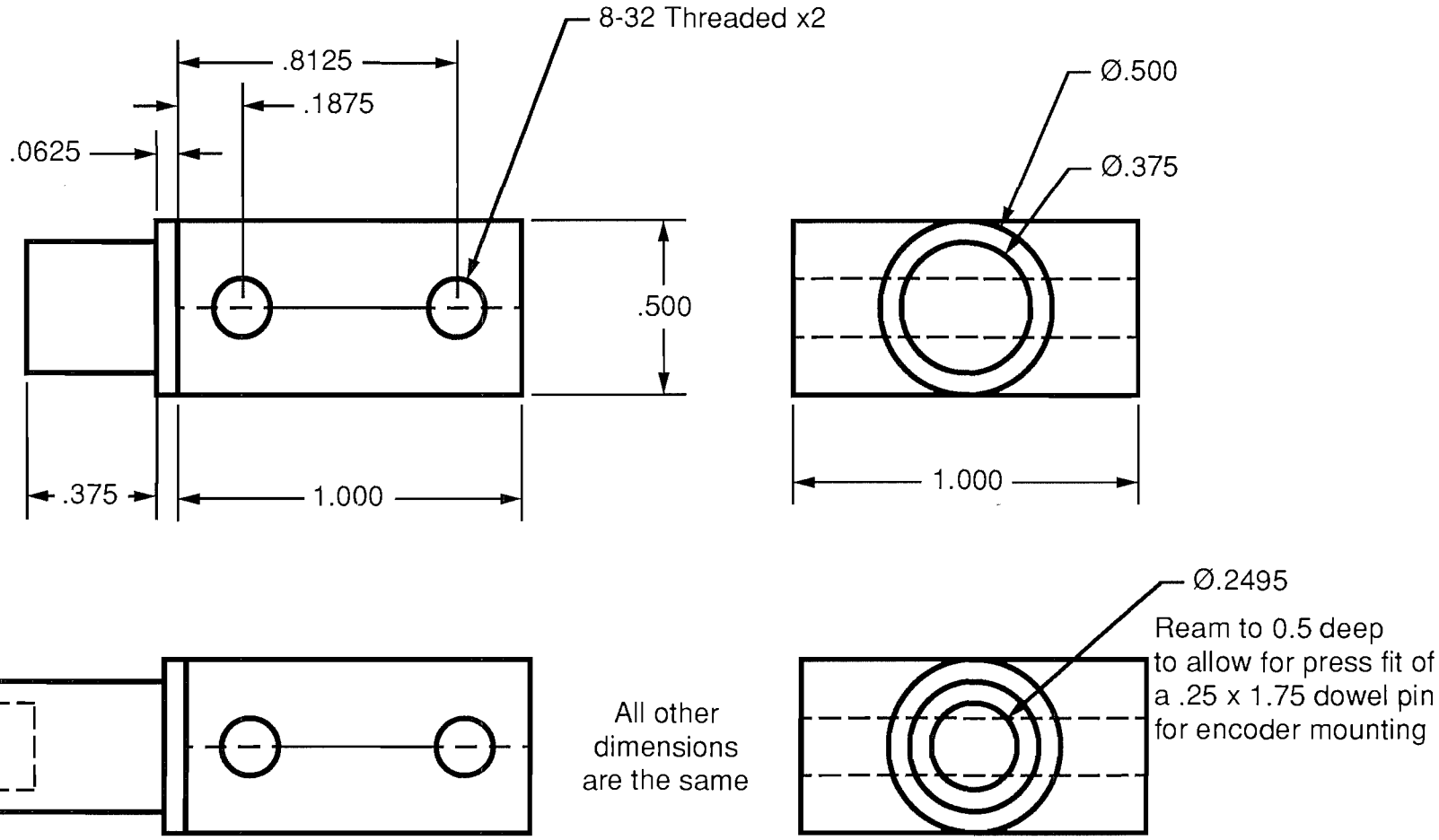

University of California, Irvine	
Department of Mechanical and Aerospace Engineering	
Robotics Lab, ELF 131 (714) 856-8051	
Pantograph Housing Shaft	
DRAWN C. Collins	QUANTITY 3 each
DATE 3/93	SCALE 2:1

Material: Aluminum

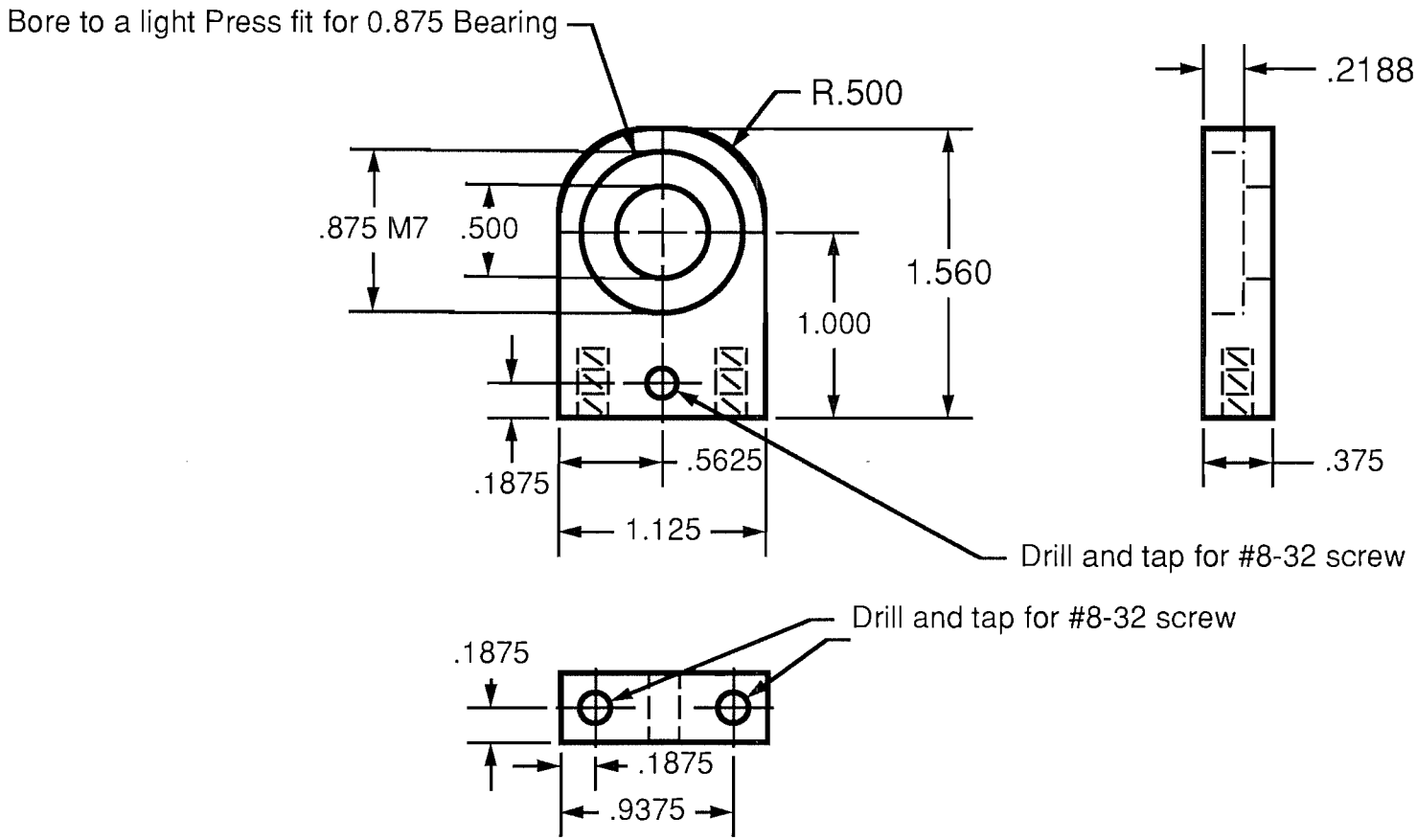

University of California, Irvine Department of Mechanical and Aerospace Engineering Robotics Lab, ELF 131 (714) 856-8051	
Pantograph Housing Support	
DRAWN C. Collins	QUANTITY 6
DATE 3/93	SCALE FULL

Material: Aluminum

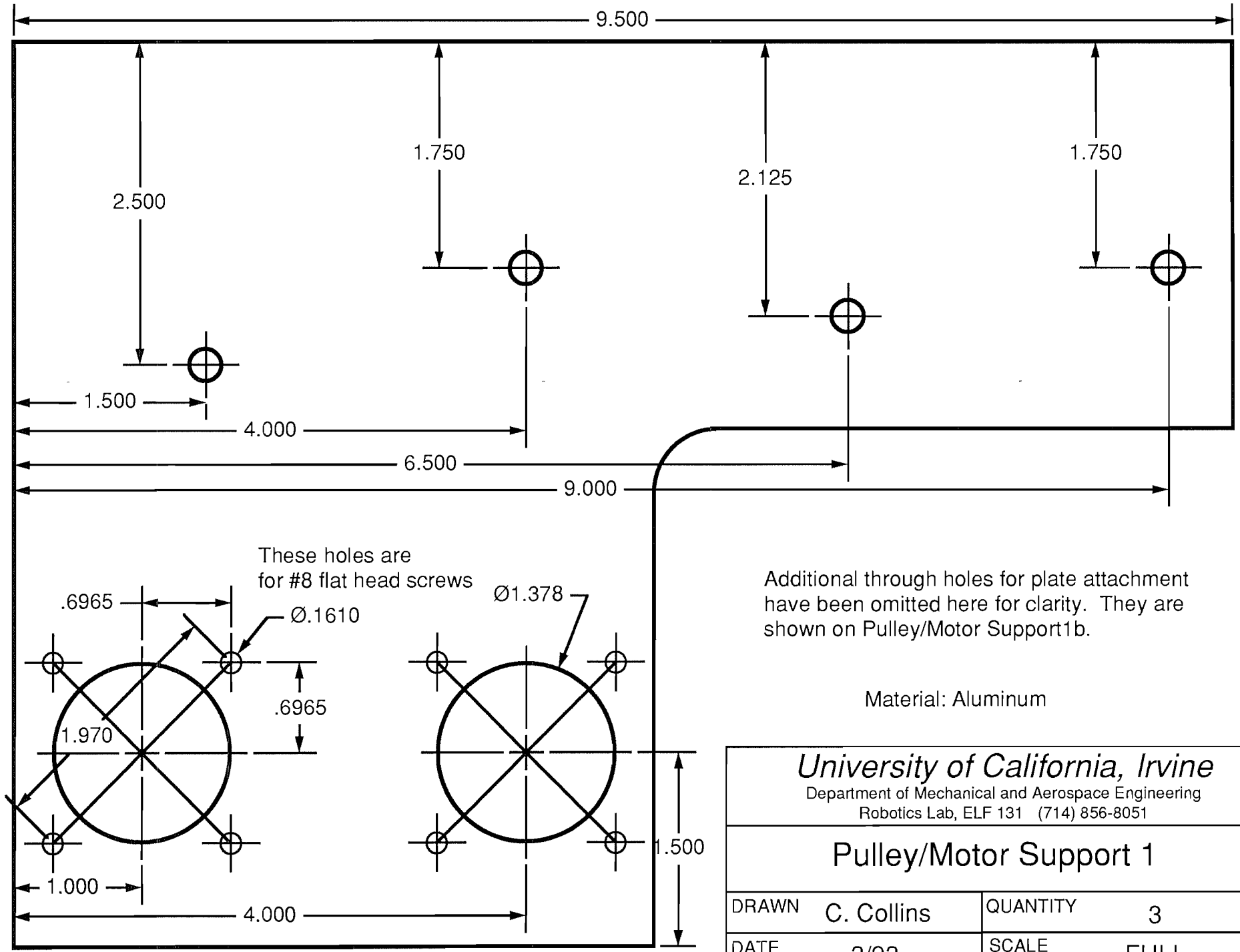

Additional through holes for plate attachment have been omitted here for clarity. They are shown on Pulley/Motor Support1b.

Material: Aluminum

University of California, Irvine
Department of Mechanical and Aerospace Engineering
Robotics Lab, ELF 131 (714) 856-8051

Pulley/Motor Support 1

DRAWN	C. Collins	QUANTITY	3
DATE	3/93	SCALE	FULL

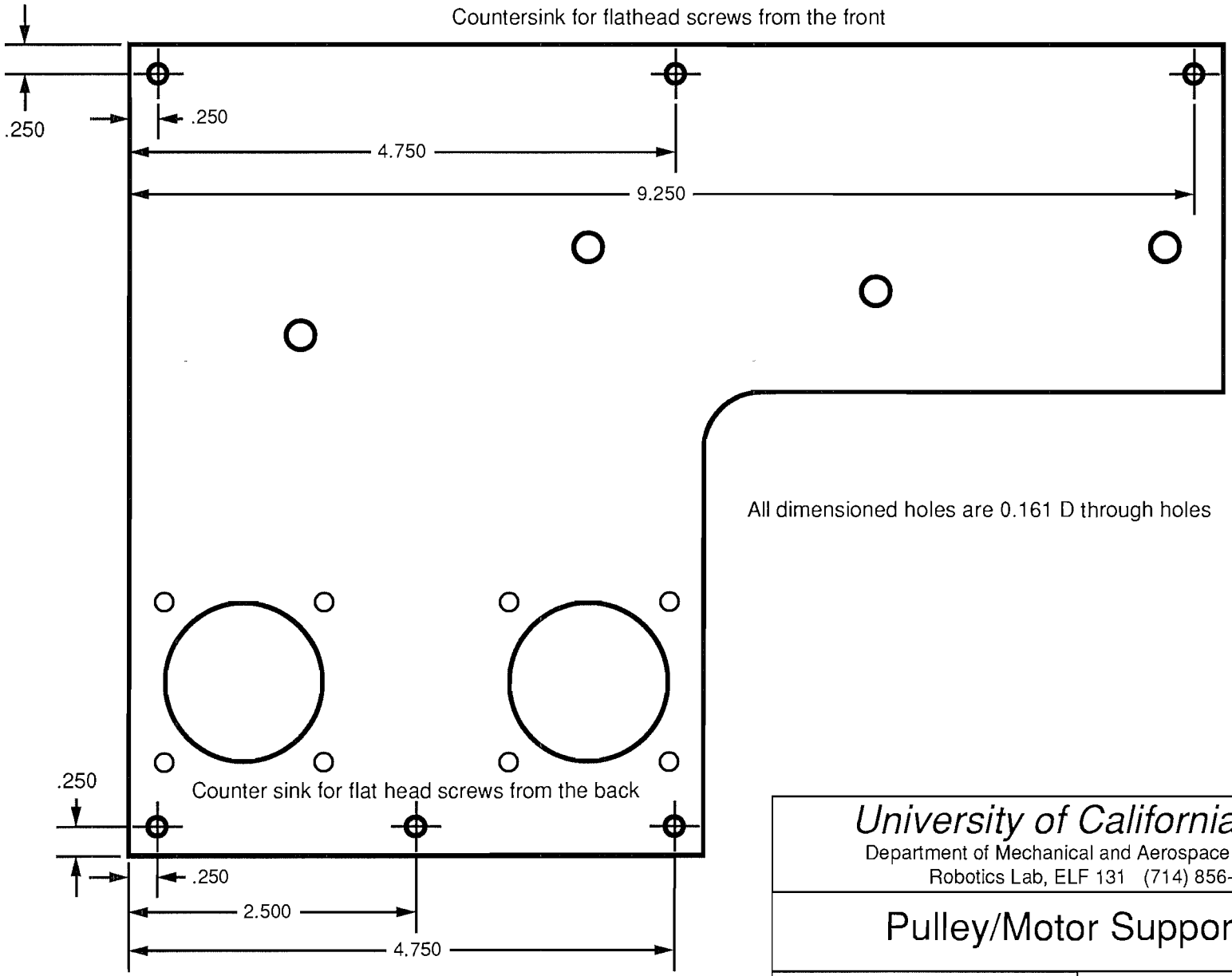

University of California, Irvine
Department of Mechanical and Aerospace Engineering
Robotics Lab, ELF 131 (714) 856-8051

Pulley/Motor Support 1b

DRAWN	C. Collins	QUANTITY	3
DATE	3/93	SCALE	3:4

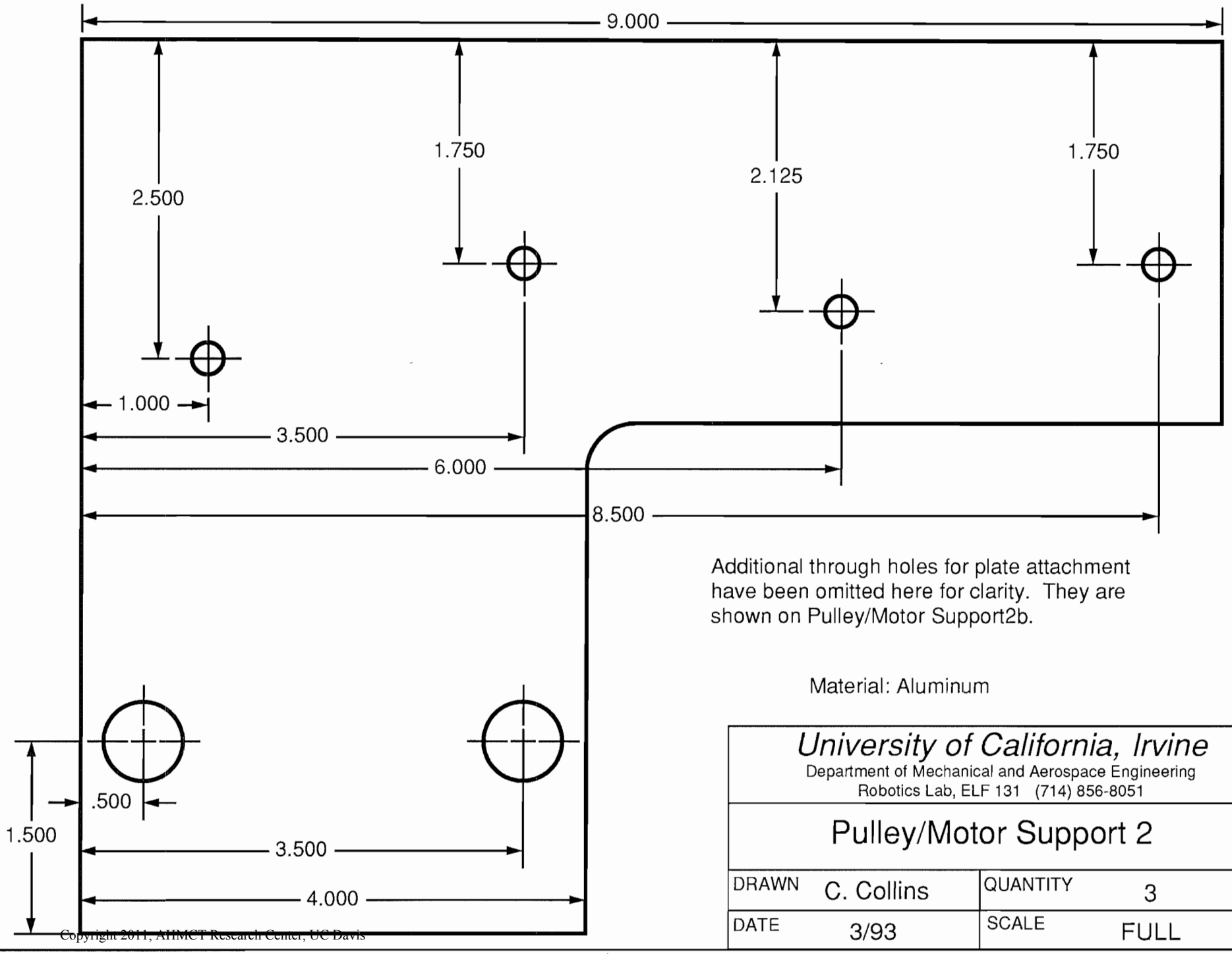

Additional through holes for plate attachment have been omitted here for clarity. They are shown on Pulley/Motor Support2b.

Material: Aluminum

University of California, Irvine	
Department of Mechanical and Aerospace Engineering Robotics Lab, ELF 131 (714) 856-8051	
Pulley/Motor Support 2	
DRAWN C. Collins	QUANTITY 3
DATE 3/93	SCALE FULL

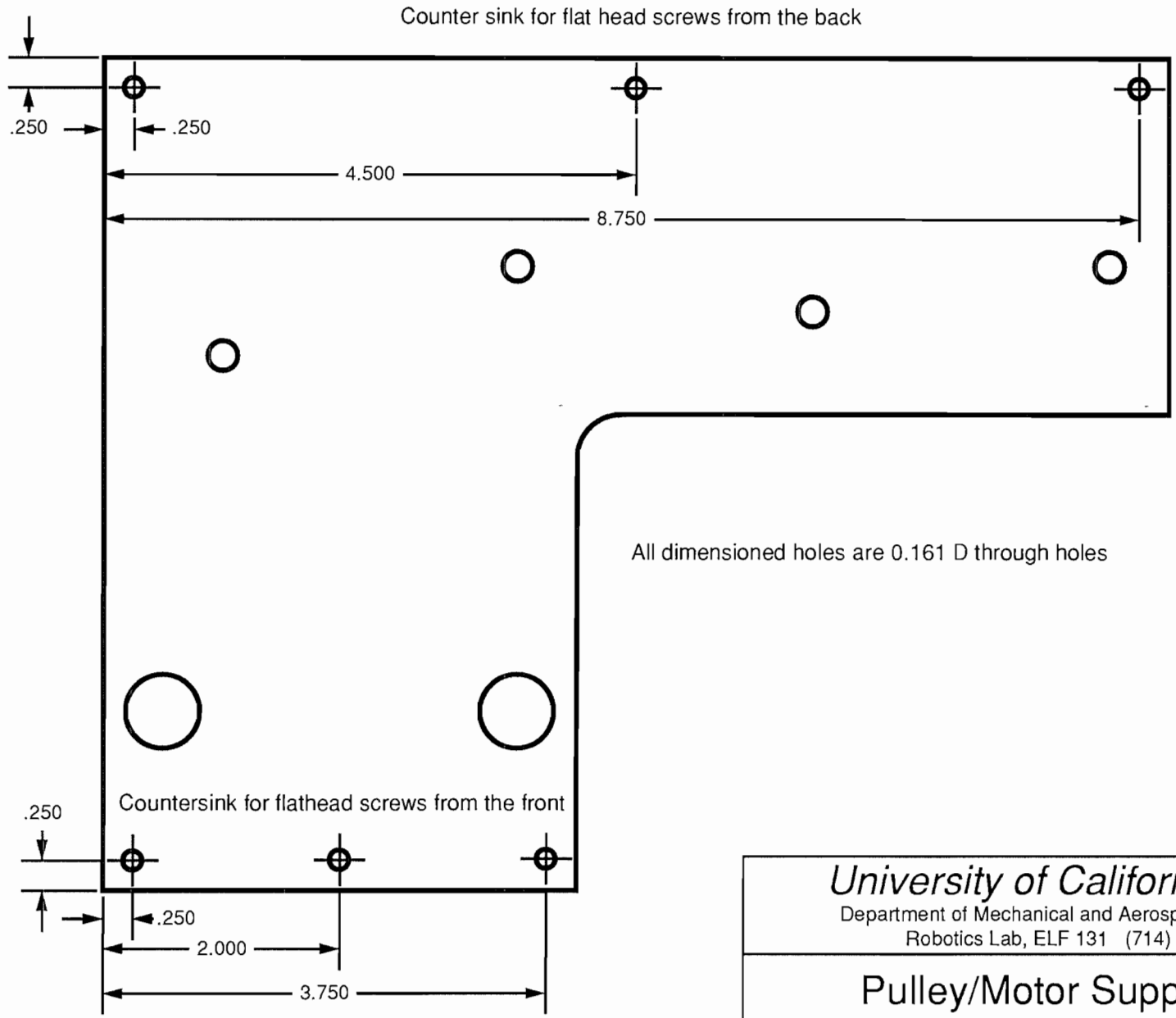

University of California, Irvine Department of Mechanical and Aerospace Engineering Robotics Lab, ELF 131 (714) 856-8051	
Pulley/Motor Support 2b	
DRAWN C. Collins	QUANTITY 3
DATE 3/93	SCALE 3:4

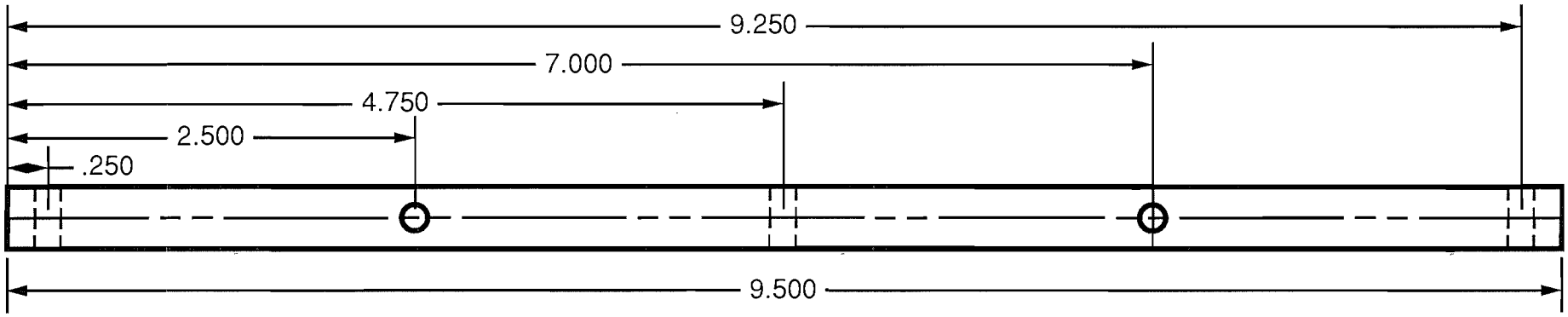

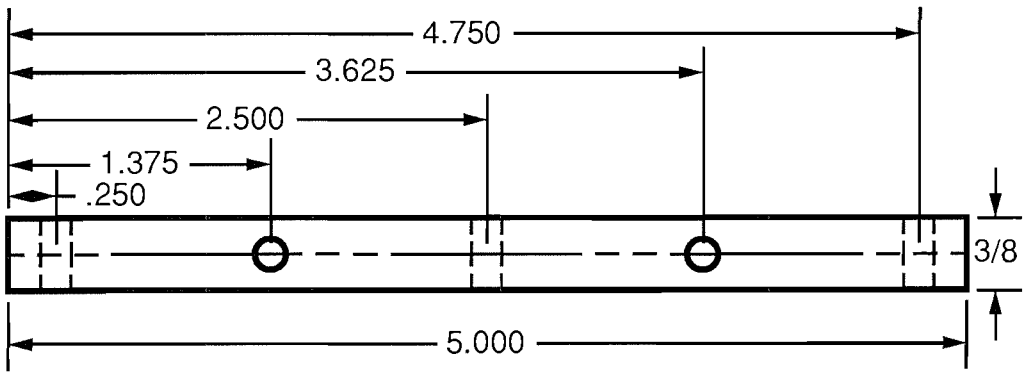

Machine from standard 1/2 x 3/8 stock.

Drill and tap all holes for #8-32 screws

University of California, Irvine
Department of Mechanical and Aerospace Engineering
Robotics Lab, ELF 131 (714) 856-8051

Screw Bars 1

DRAWN	C. Collins	QUANTITY	3ea
DATE	3/93	SCALE	–

Material: Aluminum

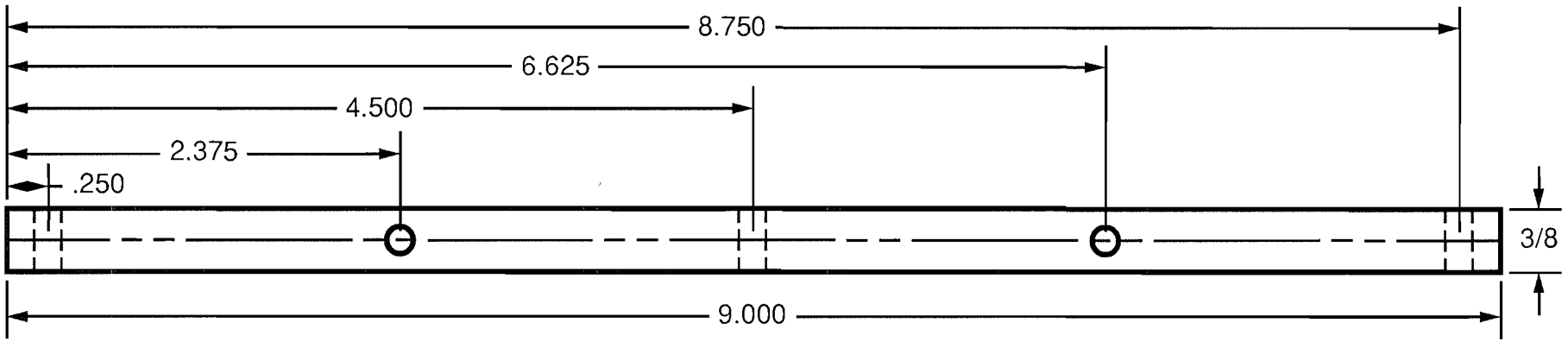

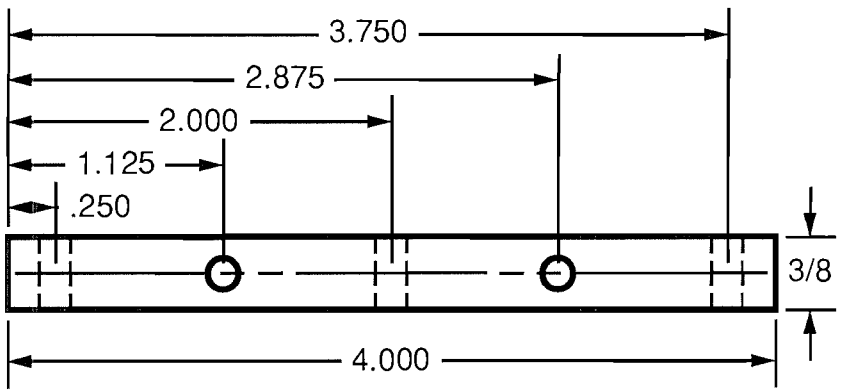

Machine from standard 1/2 x 3/8 stock.

Drill and tap all holes for #8-32 screws

University of California, Irvine Department of Mechanical and Aerospace Engineering Robotics Lab, ELF 131 (714) 856-8051	
Screw Bars 2	
DRAWN C. Collins	QUANTITY 3ea
DATE 3/93	SCALE –

Material: Aluminum

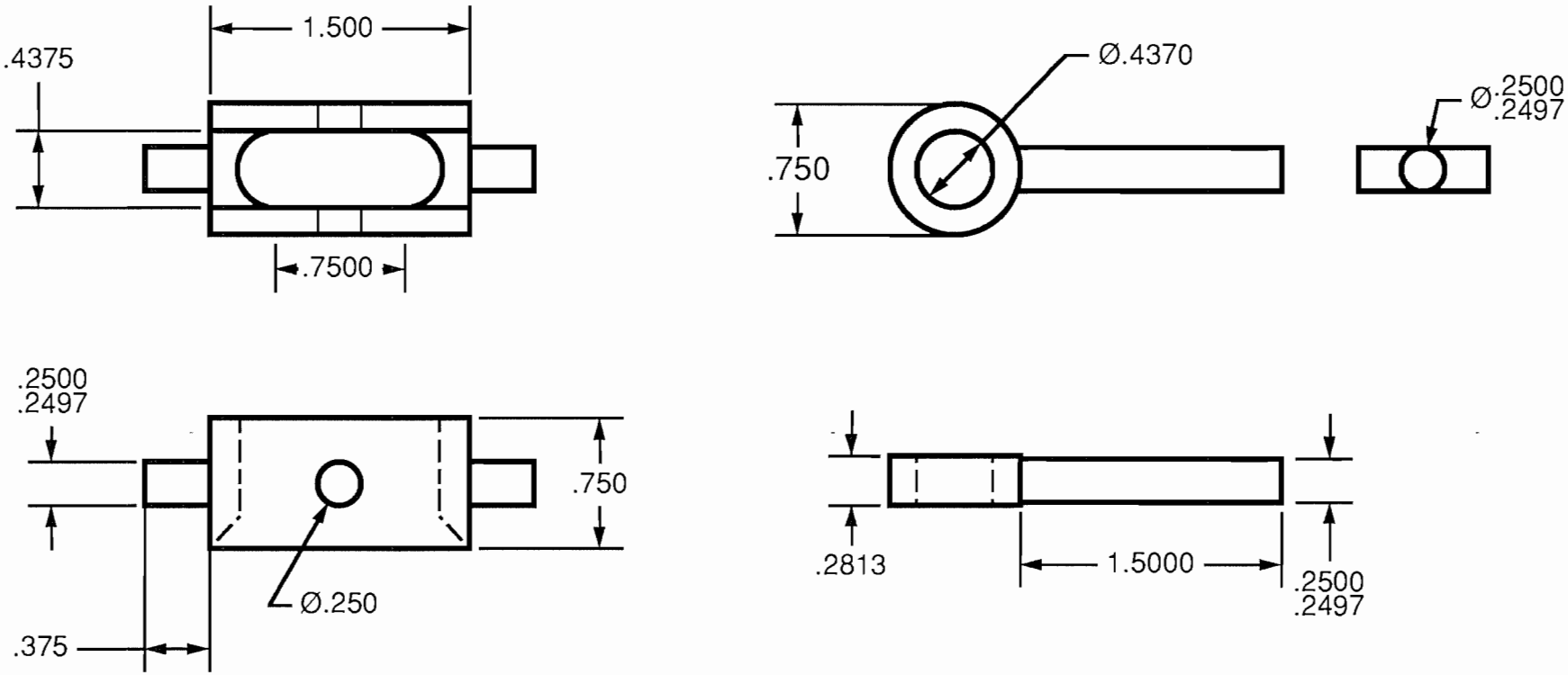

University of California, Irvine
Department of Mechanical and Aerospace Engineering
Robotics Lab, ELF 131 (714) 856-8051

Spherical Joint Set

DRAWN	C. Collins	QUANTITY	3ea
DATE	3/93	SCALE	FULL

Material: Stainless Steel

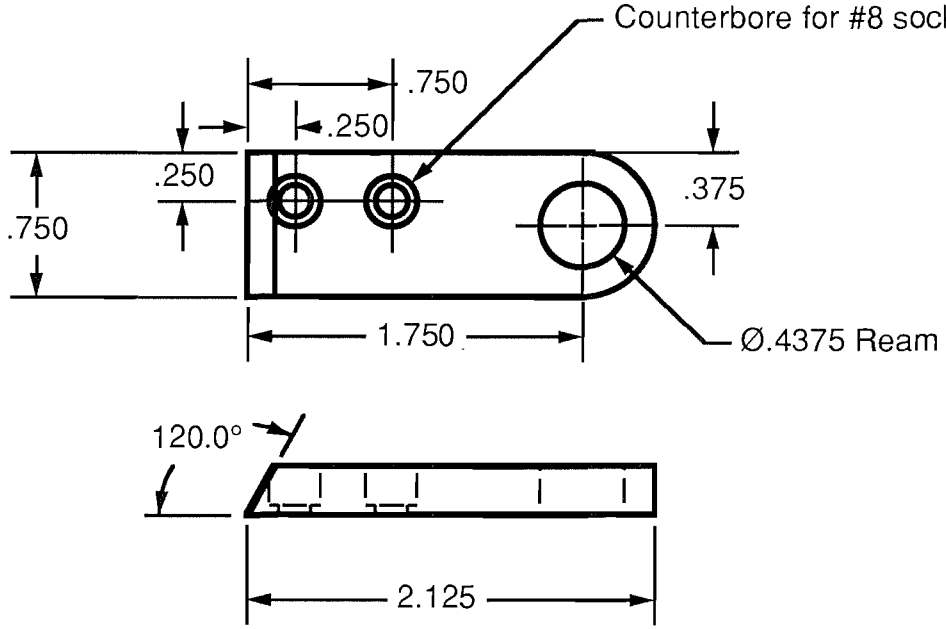

Right Side Support

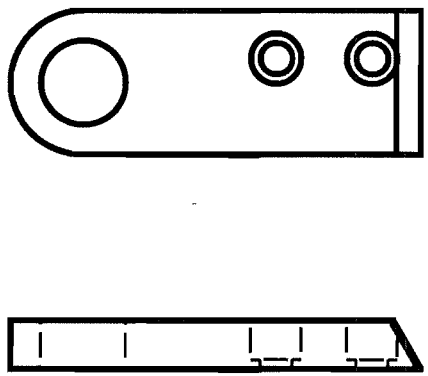

Left Side Support
Mirror Image with same dimensions

University of California, Irvine Department of Mechanical and Aerospace Engineering Robotics Lab, ELF 131 (714) 856-8051			
Spherical Joint Supports			
DRAWN	C. Collins	QUANTITY	3 each
DATE	3/93	SCALE	FULL

Material: Aluminum

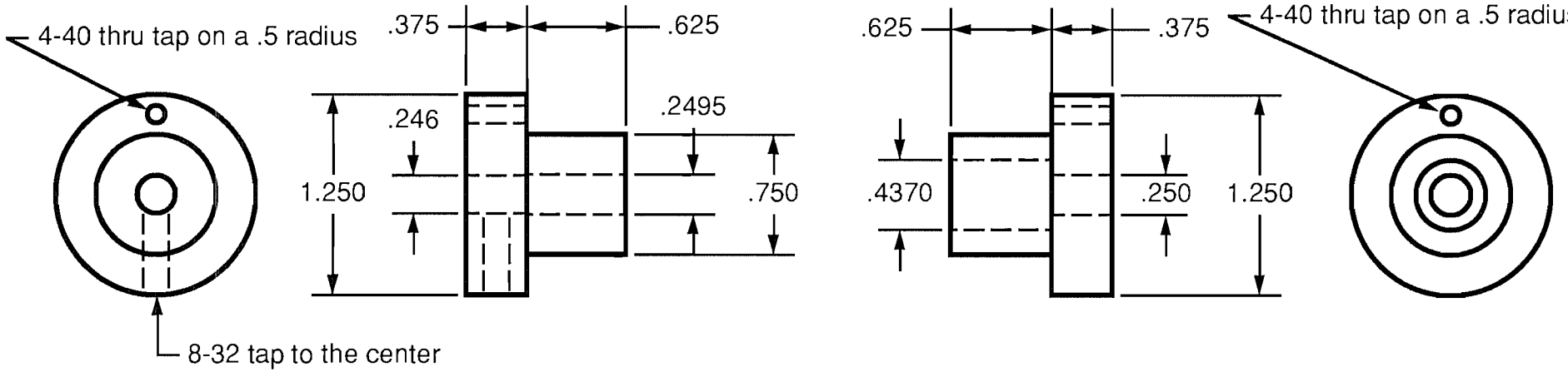

A 2" .2497 OD stainless steel shaft will be pressed into the .2495 hole providing the rolling surface for the clutch bearing.

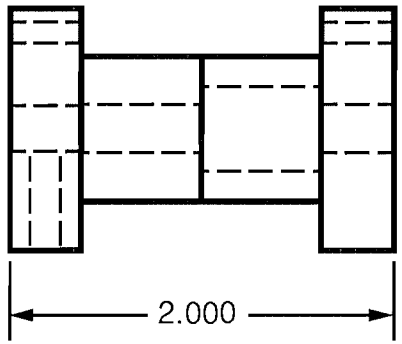

Flats can be milled on the 1.25 D portion to facilitate pretensioning

University of California, Irvine
Department of Mechanical and Aerospace Engineering
Robotics Lab, ELF 131 (714) 856-8051

Split Drive Pulley

DRAWN	C. Collins	QUANTITY	6ea
DATE	3/93	SCALE	FULL

Material: Aluminum

Mill a 1/16 wide channel 0.1 deep on a 0.5 radius as shown
Mill 1/8 wide channel 1/4 long for termination
Drill and tap for a #4 flat head screw to secure termination

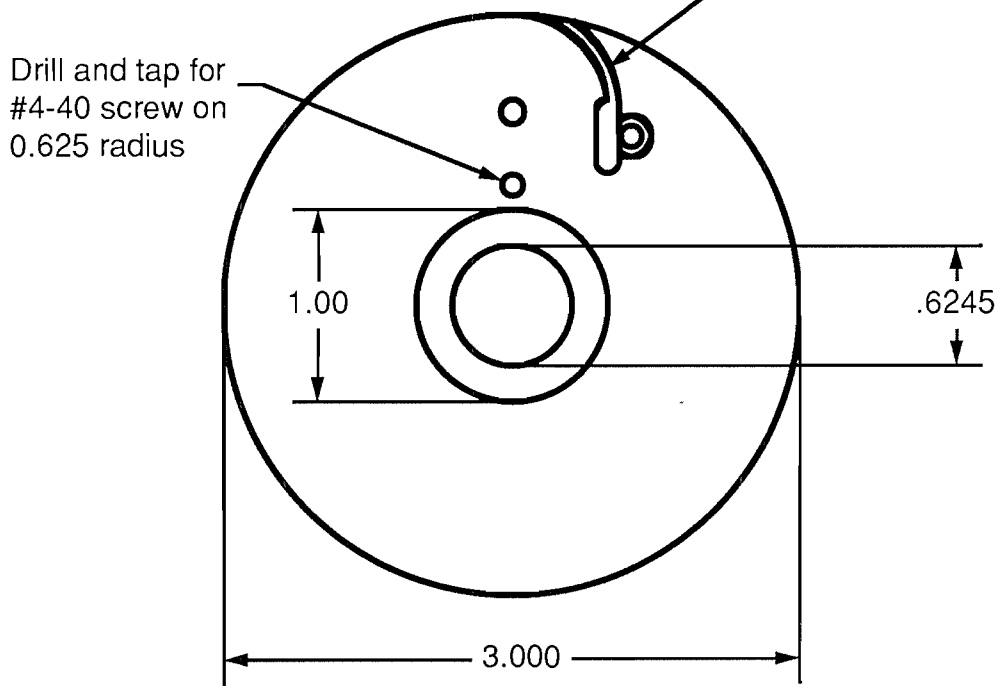

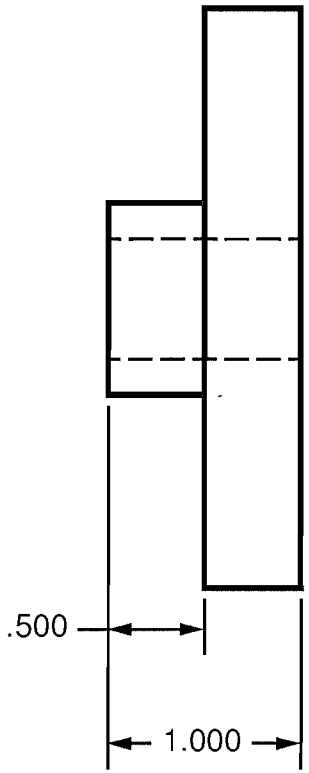

University of California, Irvine Department of Mechanical and Aerospace Engineering Robotics Lab, ELF 131 (714) 856-8051	
Stage 1 Pulley	
DRAWN C. Collins	QUANTITY 12
DATE 3/93	SCALE FULL

Material: Aluminum

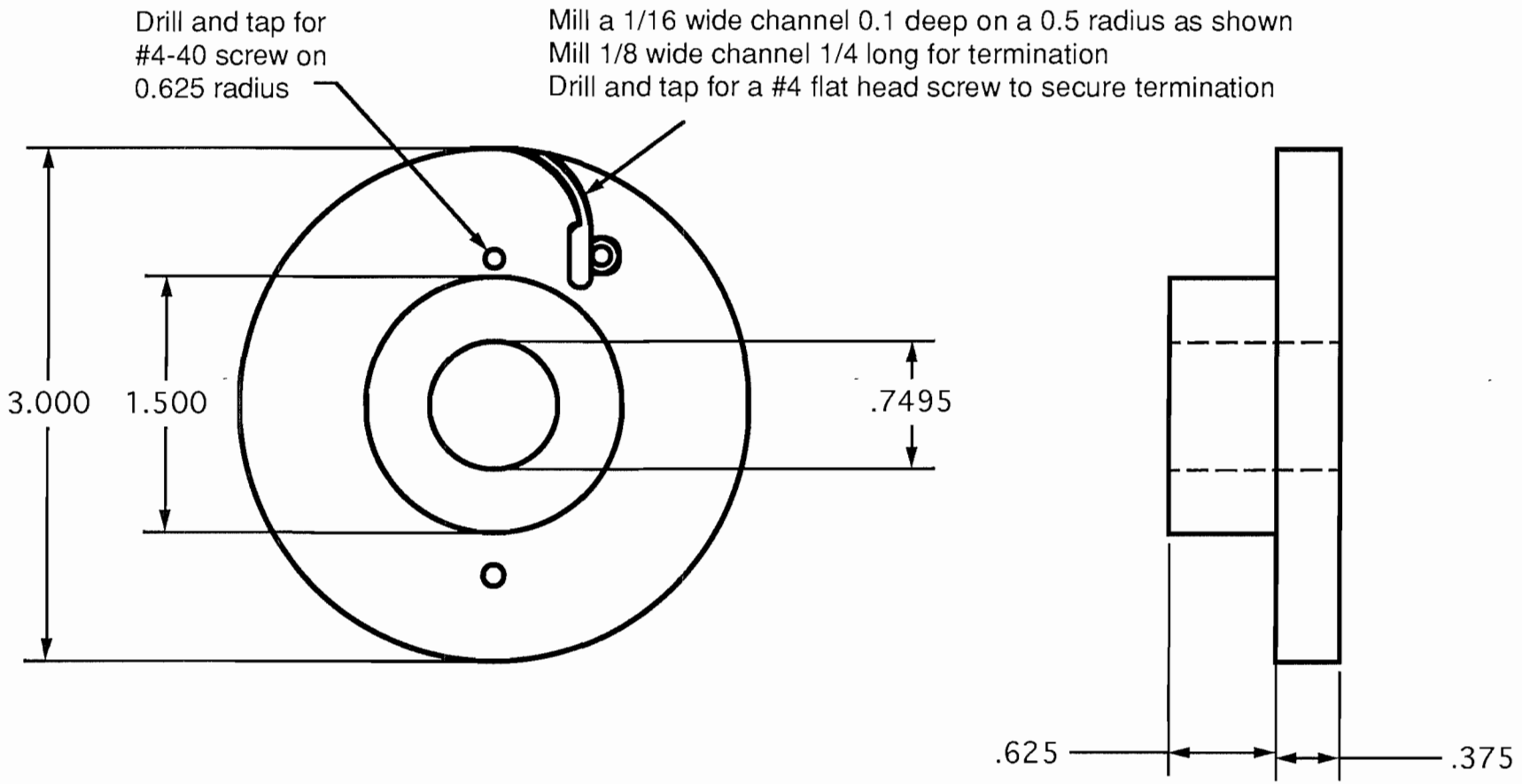

University of California, Irvine Department of Mechanical and Aerospace Engineering Robotics Lab, ELF 131 (714) 856-8051	
Stage 2 Pulley	
DRAWN C. Collins	QUANTITY 12
DATE 3/93	SCALE FULL

Material: Aluminum

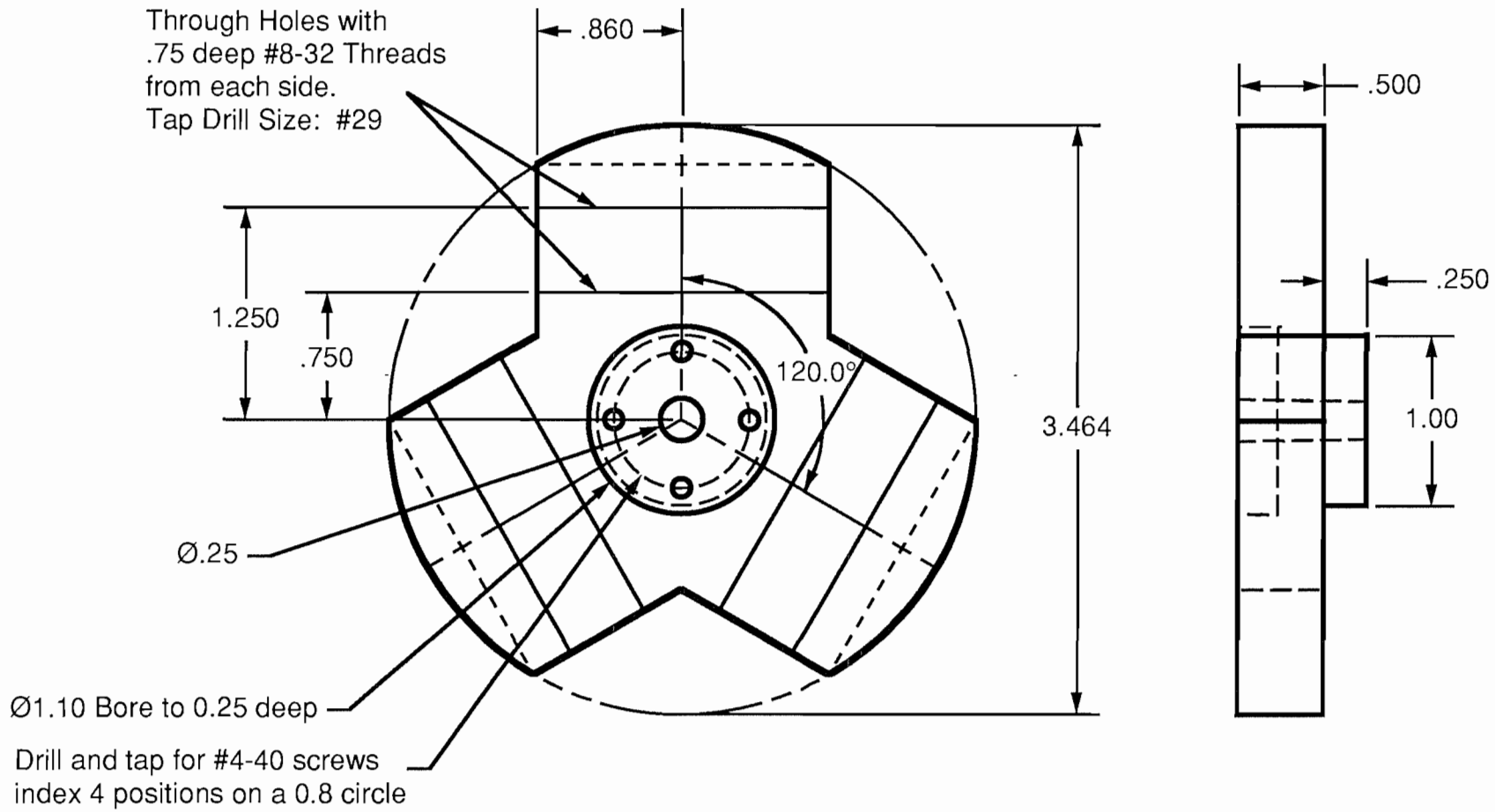

University of California, Irvine
Department of Mechanical and Aerospace Engineering
Robotics Lab, ELF 131 (714) 856-8051

Top Platform

DRAWN	C. Collins	QUANTITY	1
DATE	3/93	SCALE	FULL

Material: Aluminum

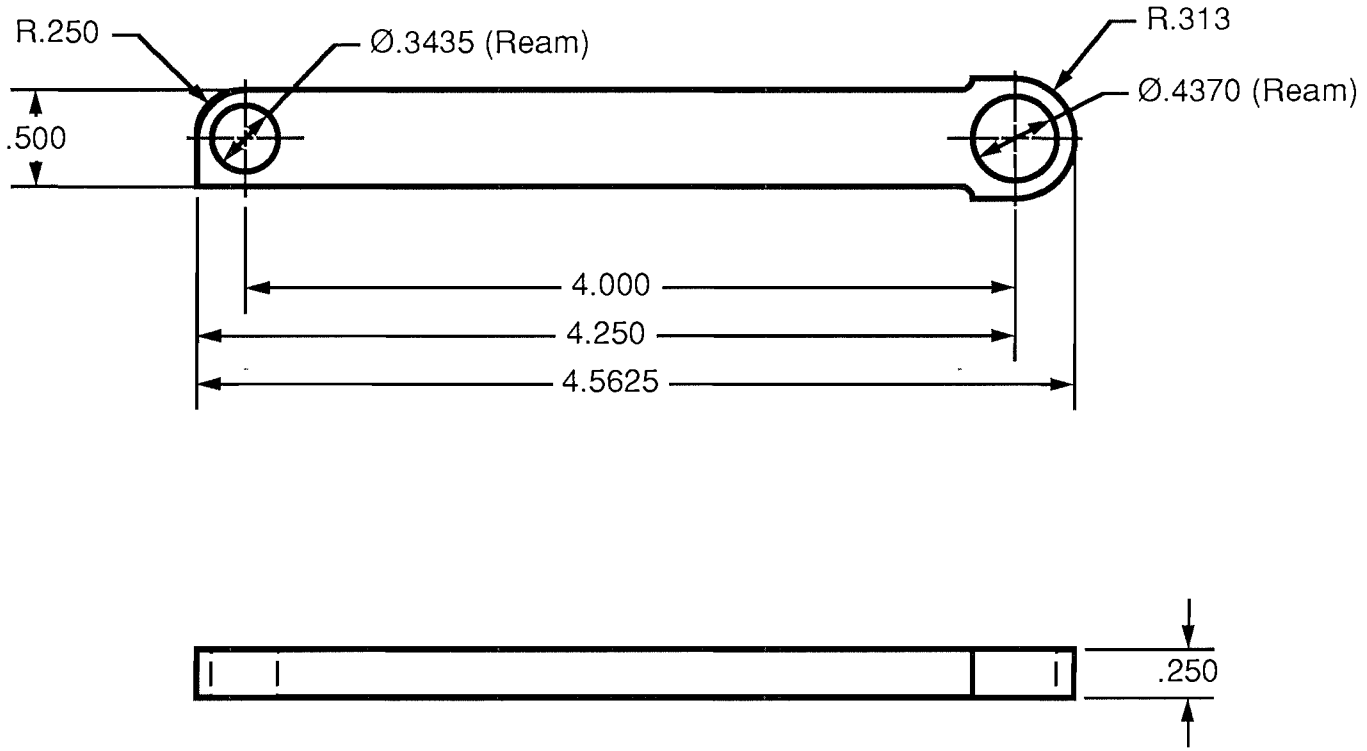

University of California, Irvine Department of Mechanical and Aerospace Engineering Robotics Lab, ELF 131 (714) 856-8051	
Upper Pantograph Link	
DRAWN C. Collins	QUANTITY 6
DATE 3/93	SCALE FULL

Material: Aluminum